

Structure and properties of the Mg alloys in as-cast state and after heat and laser treatment

L.A. Dobrzański ^{a,*}, T. Tański ^a, J. Domagała ^a, M. Król ^a, Sz. Malara ^a, A. Klimpel ^b

^a Division of Materials Processing Technology, Management and Computer Techniques in Materials Science, Institute of Engineering Materials and Biomaterials, Silesian University of Technology, ul. Konarskiego 18a, 44-100 Gliwice, Poland

^b Welding Department, Silesian University of Technology, ul. Konarskiego 18a, 44-100 Gliwice, Poland

* Corresponding author: E-mail address: leszek.dobrzanski@polsl.pl

Received 26.09.2008; published in revised form 01.12.2008

Manufacturing and processing

ABSTRACT

Purpose: The goal of this paper is to present the structure and properties of the magnesium cast alloys in as-cast state and after a heat treatment. Moreover in purpose of this paper is to extend a complex evaluation of magnesium alloys after laser surface treatment and the new methodology to determine the thermal characteristics of magnesium alloy using the novel Universal Metallurgical Simulator and Analyzer Platform (UMSA).

Design/methodology/approach: Laser treatment of magnesium alloys alloyed with TiC, SiC, WC, VC, Al₂O₃ powders was carried out using a high power diode laser (HDPL). Experiments also were performed using the UMSA.

Findings: The analysis of the thin foils after the ageing process has confirmed that the structure of the magnesium cast alloy consists of the Mg solid solution (matrix), of the secondary Mg₁₇Al₁₂ β phase – evenly located in the structure. The structure creates agglomerates in the form of needle precipitations, partially coherent with the matrix, placed mostly at the grain boundaries. The alloyed region has a fine microstructure with hard carbide particles. The structure of the alloyed zone is dendritic. Microhardness of laser alloyed surface layer with ceramic powders was significantly improved compared to alloy without laser treatment. The research of the thermal analysis shows that UMSA Technology Platform is an efficient tool for collection and calculate of thermal parameters.

Research limitations/implications: Totally there are some restriction for use of ceramic powders for alloying, some powders as oxides and nitrides are not favorable for alloying because of their dissolution during the alloying process. Further tests should be carried out in order to examine different cooling rates and parameters of solution treatment process and aging process. Investigations using the UMSA devices should concentrate on proper assessment of influence of different solidification rates on microstructure and mechanical properties.

Originality/value: The originality of this work is applying of High Power Diode Laser for alloying of magnesium alloy using hard powders and also the Universal Metallurgical Simulator and Analyzer Platform.

Keywords: Magnesium alloy; Casting; Thermal analysis; High Power Diode Laser

1. Introduction

The magnesium alloys are, apart from the titanium alloys, a very modern and of good quality material for manufacturing different machine elements and devices. Hence, the increasing interest in magnesium, also in the cognitive area, can be observed, supported by the fact of organizing big world conferences on this subject [1-4].

The greatest part of the manufactured magnesium is being used as an addition or a microaddition to the ferrous alloy or the nonferrous alloys. However, almost one third of the world's production of magnesium is mainly meant for manufacturing magnesium alloys as pressure castings. According to the statistics of *Hydro Magnesium* company, the production of the magnesium cast alloys was increasing in the years 1993-2003 in the parabolic course, up to almost 180 000 tons, and Europe significantly contributed to this increase with its 80 000 tons. The demand for the magnesium cast alloys is mainly connected with the development of the automotive industry. For example, *General Motors* in their big cars (Savana & Express) use 26,3 kg of magnesium cast alloys, and in smaller cars (Safari, Astro) – 165 kg, Ford F – 150 – 14,5 kg, VW Passat and Audi A4 and A6 from 13,6 to 14,5 kg, Alfa Romeo – 9,3kg. A further demand for

magnesium casts is expected, of up to 50 kg per each car. It is mainly because of the fact that the magnesium casts have got a low density (1700-1900 kg/m³), and at the same time, their mechanical properties are similar to the aluminium casting alloys. Magnesium alloys have got good casting properties and the possible shrinkage porosities or hot micro-cracks can be counteracted by applying alloy additions. By choosing the alloy additions, the mechanical properties or corrosion resistance can be influenced [5-8].

Magnesium alloys have also found their application in manufacturing of mowers, saws, robots, office equipment including computer hardware, sport and medical appliances, in production of movie and video cameras, for rocket parts, space ships, and others (Table 1.) [9].

The growing trends in the production of magnesium alloys point at the increased necessity of their application in the world constructional industry, and the magnesium alloys will become one of the most frequent materials used in the following decades. Hence, it is so extremely important to maintain a high pace of the research over the issue of the light alloys, including also that done in the Division of Materials Processing Technology, Management and Computer Techniques, in Materials Science of the Institute of Engineering Materials and Biomaterials of Silesian University of Technology.

Table 1.
Areas of application / Spectrum of parts from magnesium alloys [1-9]

Power Tools	
housings and various components of drilling machines, power saws, accu screw drivers, power hammers, chain saws, riveting systems	
Automotive	
Powertrain	housings (gearbox, electric motors, hydraulic elements), cylinder head covers, brockets, cross-beams
Safety Systems	steering wheel columns, steering wheel skeletons, airbag housings
Chassis & Car body	body elements, fixation elements, accessory elements, decorative parts (outside)
Interiors	cockpit cross-beams, dashboard elements, door handles, knobs, switches
Consumer Electronics	
Laptops	frames, shells, covers and shielding elements
Mobile Phones	shells, hinges, LCD frames, shielding elements
Loudspeakers	membranes
LCD	frames
PDA, GPS	housings
Others	
Civil Aviation	seating elements, cockpit structures
Sports	bicycle components, motorbike components
Buildings	decorative, electroplated applications, door handles and knobs
Armament	canisters for ammunition, housings of communication system

In order to effectively control microstructure development during the melting, solidification as well as further materials processing is necessary to understand all metallurgical phenomena taking place. Knowledge of the solidification process as well as the influence of liquid and/or semi solid metal treatment on micro and macro structure characteristic is of primary importance. The simple and very effective method, which make it possible to determine a curve of the crystallization process – the cool curve $T=F(t)$, is thermal analysis. Advanced Thermal Analysis (TA) techniques monitor the temperature changes in sample as it cools through a phase transformation interval. The temperature changes in the materials are recorded as a function of the heating or cooling time in such a manner that allows for the detection phase transformation. In order to increase accuracy, characteristic points on the cooling curve have been identified using the first derivative curve plotted versus time [10-16].

In the metal casting industry, an improvement of component quality depends mainly on better control over the production parameters. Thus, computer aided cooling curve thermal analysis of alloys is used extensively for the evaluation of several processing and material parameters. Thermal analysis of alloys can provide information about composition of the alloy, the latent heat of solidification, the evolution of fraction solid, the types of phases that solidify and even dendrite coherency. There are also many other uses for TA such as determining dendrite arm spacing, degree of modification and grain refining in aluminum alloys, the liquidus and solidus temperatures, characteristic temperatures related to the eutectic regions and intermetallic phase formation [17-23].

A lot of light metal applications require a special properties of material surface layer. Method which allow to achieve improvement of the chemical, mechanical and tribological properties of the surfaces is a high power laser treatment. There are several laser surface treatments, namely surface hardening, alloying, cladding and laser melt injection. In surface hardening, the laser beam heats the work piece and changes the microstructure in such a way that the surface properties, for example hardness, of the work piece are changed. In laser alloying the laser beam melts the surface locally while a second material is added to the melt pool. After rapid solidification, the composition, the morphology and properties on the top layer of the workpiece is changed. The aim of laser cladding is the deposition of a cladding onto surfaces of work pieces. The material is deposited by pre-placed powder, powder injection or by wire feeding. The laser beam melts a thin layer of the surface of the work piece together with additional material. After solidification, a small mixture of the top part of the work piece and the coating provides the bonding between substrate and coating. In the laser melt injection process, solid particles are injected in the melt pool, which are trapped after solidification [24, 25].

All three methods involve the formation of a melt pool to which material is applied. Depending on the achieved degree of mixing between the additional material and the substrate in the surface layer, one can distinguish laser alloying and laser dispersing on the one hand, and laser cladding on the other hand. Laser alloying is characterised by a complete mixing and/or reaction of the additional elements with the base material. In contrast, laser cladding generates a surface layer that hardly

contains elements of the substrate on top of the base material. A cladding material with the desired properties is fused onto a substrate by means of a laser beam. The mixing between the clad material and base material must be as small as possible to utilise the properties of the coating material most effectively. By improving a technical surface locally with a dedicated material, one can use an ordinary cheap base material for the surface that is not being exposed to high loads [26].

The goal of this paper is presentation of the investigation results of the MCMgAl12Zn1, MCMgAl9Zn1, MCMgAl6Zn1, MCMgAl3Zn1 casting magnesium alloy in its as-cast state and after heat treatment and also after laser treatment. Besides, this investigation presents the new methodology to determine the thermal characteristics of magnesium alloy based on customized UMSA computer controlled rapid solidification experimentz.

2. Experimental procedure

The investigations have been carried out on test pieces of MCMgAl12Zn1, MCMgAl9Zn, MCMgAl6Zn1, MCMgAl3Zn magnesium alloys in as-cast and after heat treatment states made in cooperation with the Faculty of Metallurgy and Materials Engineering of the Technical University of Ostrava and the CKD Motory plant, Hradec Kralove in the Czech Republic. The chemical compositions of the investigated materials are given in Table 2. A casting cycle of alloys has been carried out in an induction crucible furnace using a protective salt bath *Flux 12* equipped with two ceramic filters at the melting temperature of $750\pm 10^\circ\text{C}$, suitable for the manufactured material. In order to maintain a metallurgical purity of the melting metal, a refining with a neutral gas with the industrial name of *Emgesalem Flux 12* has been carried out. To improve the quality of a metal surface a protective layer *Alkon M62* has been applied. The material has been cast in dies with betonite binder because of its excellent sorption properties and shaped into plates of $250\times 150\times 25$. The cast alloys have been heated in an electrical vacuum furnace *Classic 0816 Vak* in a protective argon atmosphere.

Table 2.
Chemical composition of investigation alloy

The mass concentration of main elements, %						
Al	Zn	Mn	Si	Fe	Mg	Rest
12.1	0.62	0.17	0.047	0.013	86.96	0.0985
9.09	0.77	0.21	0.037	0.011	89.79	0.0915
5.92	0.49	0.15	0.037	0.007	93.33	0.0613
2.96	0.23	0.09	0.029	0.006	96.65	0.0361

The experiments were performed using a pre-machined cylindrical test sample with a diameter of $\varnothing=18\text{mm}$ and length of $l=20\text{mm}$ taken from the ingot (Fig. 1). In order to assure high repeatability and reproducibility of the thermal data, the test sample mass was $\approx 9\text{g}$. Each sample had a predrilled hole to accommodate a supersensitive K type thermocouple (with extra low thermal time constants) positioned at the centre of the test sample to collect the thermal data and control the processing temperatures.

Table 3. Characteristic points obtained from thermal-derivative analysis

Point	Temperature	Time	Description
I	T_N	t_N	Nucleation of α -phase (liquidus temperature)
II	T_{Dmin}	t_{Dmin}	The α -Mg dendrite minimum (undercooling) temperature
III	T_{DKP}	t_{DKP}	Coherency point
IV	T_G	t_G	The α -Mg dendrite growth temperature
V	$T_{(Mg+Si+Al+Mn)}$	$t_{(Mg+Si+Al+Mn)}$	Crystallization of α -Mg, Mg_2Si and phases contains Al and Mn
VI	$T_{(Mg+Si+Al+Mn)f}$	$t_{(Mg+Si+Al+Mn)f}$	End of crystallization of Mg_2Si and phases contains Al and Mn
VII	$T_{E(Mg+Al)N}$	$t_{E(Mg+Al)N}$	Beginning of nucleation of $\alpha(Mg)$ - $\beta(Mg-Mg_{17}Al_{12})$ eutectic
VIII	$T_{E(Mg+Al)min}$	$t_{E(Mg+Mg_{17}Al_{12})min}$	The $\alpha(Mg)$ - $\beta(Mg-Mg_{17}Al_{12})$ minimum (undercooling) temperature
IX	$T_{E(Mg+Al)G}$	$t_{E(Mg+Al)G}$	The $\alpha(Mg)$ - $\beta(Mg-Mg_{17}Al_{12})$ eutectic growth temperature
X	T_{sol}	t_{sol}	End of solidification (solidus temperature)

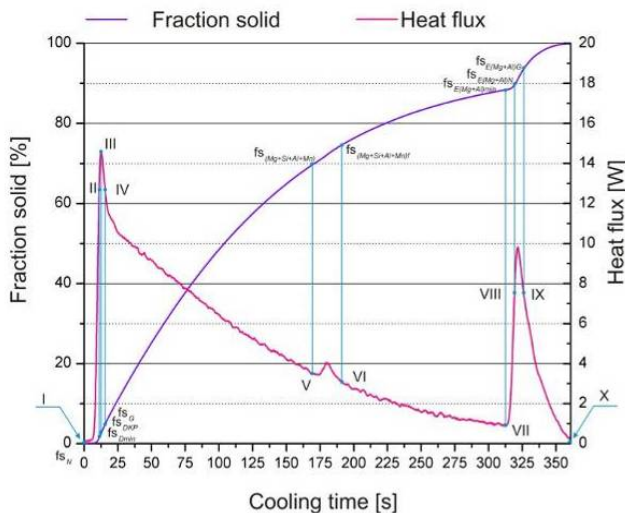


Fig. 3. Representative curves illustrate changes of heat flux and fraction solid of MC MgAl9Zn1 alloy

The heat treatment involved the solution heat treatment (warming material in temperature 375 °C the 3 hours, it later warming in the temperature to 430° C, holding for 10 hours) and cooling in air and then ageing at temperature of 190°C and cooling in air (Table 4).

Next, MCMgAl12Zn1, MCMgAl9Zn, MCMgAl6Zn1, MCMgAl3Zn1 magnesium alloys were used as substrate materials to laser surface treatment using high power diode laser. Laser surface alloying made in cooperation with Welding Department of the Silesian University of Technology in Gliwice. Laser surface alloying was conducted by remelting MCMgAl12Zn1, MCMgAl9Zn, MCMgAl6Zn1, MCMgAl3Zn surface and feeding of hard carbide particles and oxide aluminium.

The alloying materials were TiC, SiC, WC, VC, Al₂O₃ powders (Fig. 4). The powders was supplied by side injection rate of 7±1 g/min (for WC, TiC, VC powders), 8÷9 g/min for SiC particles and Al₂O₃ - 4÷5 g/min.

The laser alloying was performed by high power laser diode HPDL Rofin DL 020 under an argon shielding gas. Argon was used during laser re-melting to prevent oxidation of the surface layer and the substrate. The process parameters

during the present investigation were: laser power – 1.2 ÷ 1.6 kW, scan rate - 0.5 ÷ 1.0 m/min.

Table 4. Parameters of heat treatment of investigation alloy

Sing the state of heat treatment	Conditions of solution heat treatment		
	Temperature, °C	Time of warming, h	Cooling way
0			As-cast
Solution treatment			
1	430	10	Water
2	430	10	Air
3	430	10	In furnace
Aging treatment			
4	190	15	Air

The observations of the investigated cast materials have been made on the light microscope LEICA MEF4A as well as on the electron scanning microscope Opton DSM-940.

The X-ray qualitative and quantitative microanalysis and the analysis of a surface distribution of cast elements in the examined magnesium cast alloy specimens in as-cast and after heat, laser treatment have been made on transverse microsections on the Opton DSM-940 scanning microscope with the Oxford EDS LINK ISIS dispersive radiation spectrometer at the accelerating voltage of 15 kV and on the JEOL JCXA 733 x-ray microanalyzer.

Observations of thin foil structure were carried out in the JEM 3010UHR JEOL transmission electron microscope using an accelerating voltage of 300 kV.

Phase composition and crystallographic structure were determined by the X-ray diffraction method using the XPert device with a cobalt lamp, with 40 kV voltage. The measurement was performed in angle range of 2 θ : 20° - 130°.

Hardness tests were made using Zwick ZHR 4150 TK hardness tester in the HRF scale. Tensile strength tests were made using Zwick Z100 testing machine.

Microhardness of the cross section of the laser surface melted layer was measured on Fully-Automatic Microhardness Testing System with a loading time of 15 s and the testing load of 50 g.

The wear resistance test of cast magnesium alloys in meat-metal system was carried out with a help of tool, which was designed in Institute of Engineering Materials and Biomaterials, Silesian University of Technology (Fig. 5). The investigation were performed with a stable cycle numbers 5000 (120 m), with different loads 6, 8, 10 12 N.

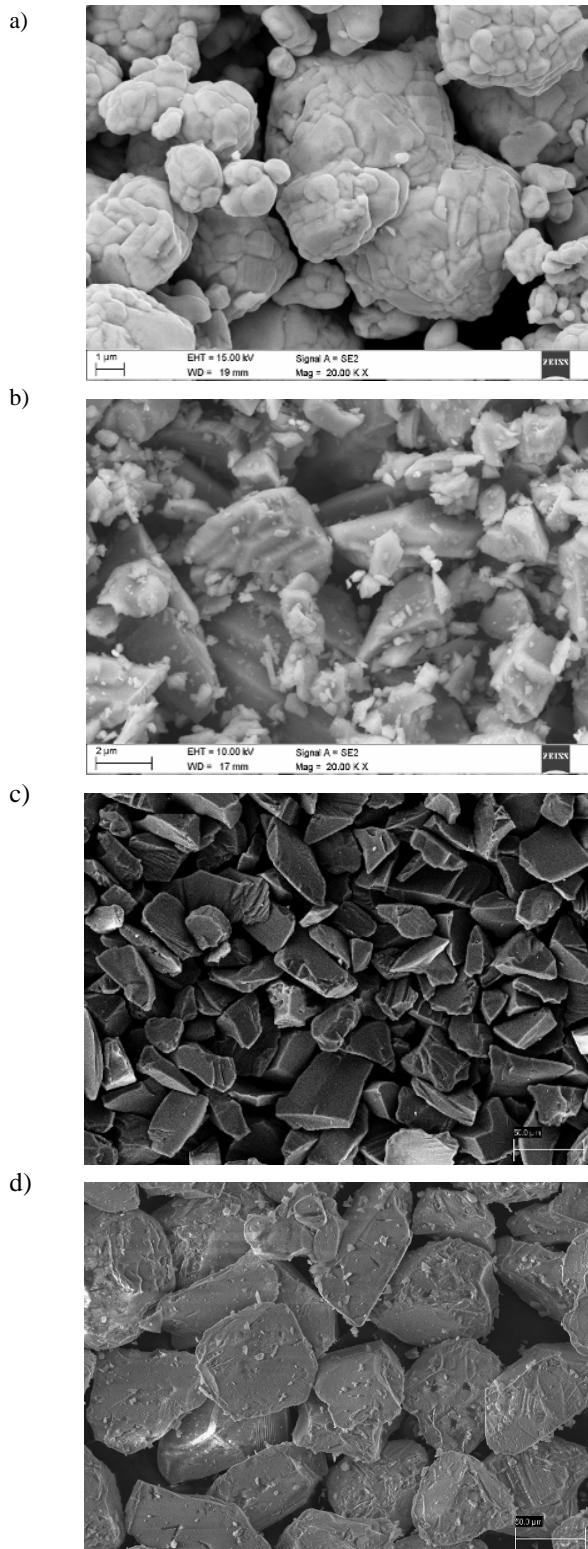


Fig. 4. Morphology of a) tungsten carbide, b) titanium carbide, c) silicon carbide powder

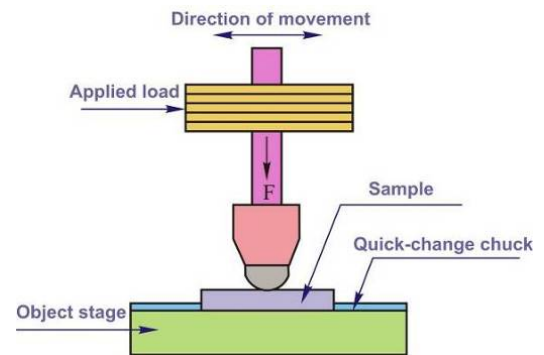


Fig. 5. Pictorial diagram to the abrasive wear investigations in a metal-metal system

For comparison of the achieved results on the basis of the performed investigations a computer neural network model was used for analysis of the aluminium content and heat treatment parameters influence on the properties of the worked out cast magnesium alloys.

As the basic coefficients for evaluation of the model quality following values were used:

- average network forecast error,
- ratio of standard deviations of errors and data,
- Pearson's correlation coefficient.

For data analysis four neural networks models were used:

- multilayer perceptron MLP,
 - linear neural networks,
 - radial basis functions neural network RBF,
 - generalized regression neural networks GRNN,
- also the following learning methods:
- back propagation method,
 - conjugate gradient,
 - quasi-Newton method,
 - fast propagation.

The applied neural networks allow to work out of a interdependence model for:

- aluminium content, temperature and solution treatment time, cooling medium, and hardness,
- aluminium content, temperature and ageing time, cooling medium, and hardness.

3. Discussion of experimental results

3.1. Thermal-derivative analysis

The general microstructure after thermal analysis revealed the presence of dendrite of solid solution of Al in Mg (α -phase) and divorced eutectic structure made of Al-rich Mg solid solution and $Mg_{17}Al_{12}$ (β -phase). Moreover, angular particles of Mg_2Si and globular particles of phases contains Al Mn mainly located at interdendritic spaces were observed (Fig. 6). This observation was in agreement with thermal analysis experiments where two distinct metallurgical reactions were noted on the cooling curve, i.e., nucleation of the $\alpha(Mg)$ and the $\alpha(Mg)$ - $\beta(Mg_{17}Al_{12})$ eutectic.

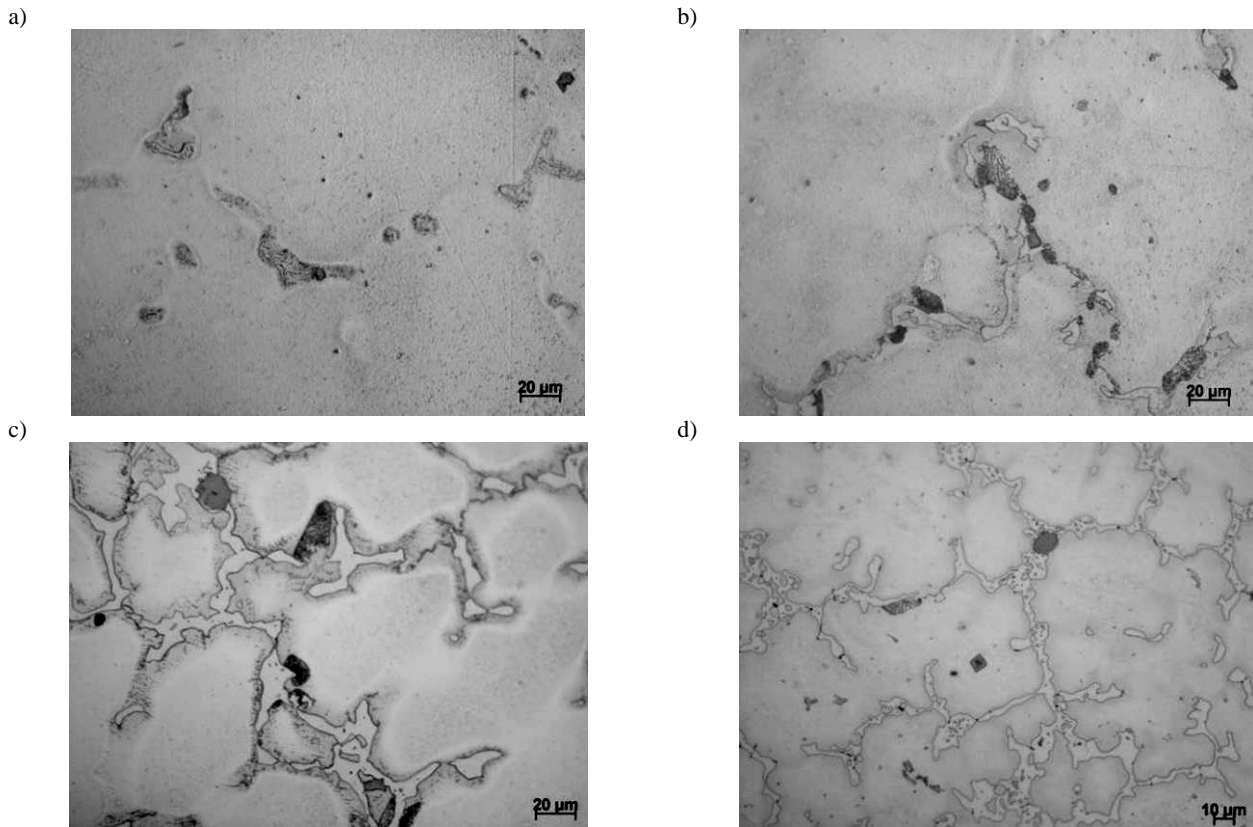


Fig. 6. Microstructure of magnesium alloys after thermal analysis: a) MC MgAl₃Zn₁, b) MC MgAl₆Zn₁, c) MC MgAl₉Zn₁, d) MC MgAl₁₂Zn₁ (x 500)

The quantitative micro analysis made on the transverse microsections of the magnesium alloys using the EDS system confirmed the evident concentrations of magnesium, silicon, aluminium and manganese what suggests the occurrence of precipitations containing Mg and Si with angular contours in the alloy structure as well as phases with high Mn and Al concentrations that are irregular often occurring in the forms of blocks or needles (Fig. 7-8).



Fig. 7. SEM micrographs of MC MgAl₃Zn₁

Table 5. Pointwise chemical composition analysis from Fig. 7

Analysis	Element	The mass concentration of main elements, %	
		weight	atomic
1	Zn	06.35	02.53
	Al	68.10	72.85
	Mg	25.55	24.62
2	Mg	3.82	5.9
	Al	40.06	55.74
3	Mn	56.13	38.36
	Mg	68.98	71.98
	Si	31.02	28.02

Because the size of particular elements of the structure is, in a prevailing measure, smaller than the diameter of the analyzing beam, the obtained at the quantitative analysis chemical composition may be averaged as a result of which some values of element concentrations may be overestimated.

Thermal analysis of the magnesium alloys have been presented on Figure 9. Two visible temperature arrests were noted on the cooling curves. More detailed information pertaining to the alloy's thermal characteristics such as non-equilibrium liquidus, nucleation of the $\alpha(\text{Mg})$ - $\beta(\text{Mg}_{17}\text{Al}_{12})$ eutectic, etc. were determined using the first derivative curves.

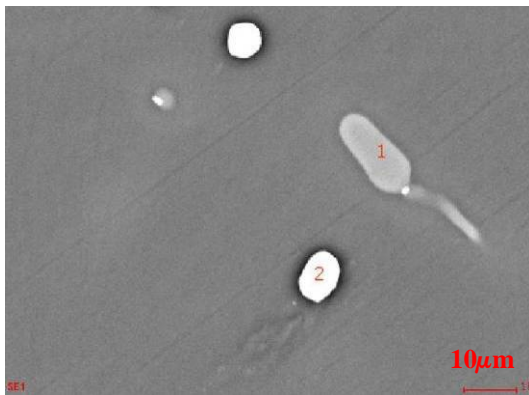


Fig. 8. SEM micrographs of MC MgAl9Zn1

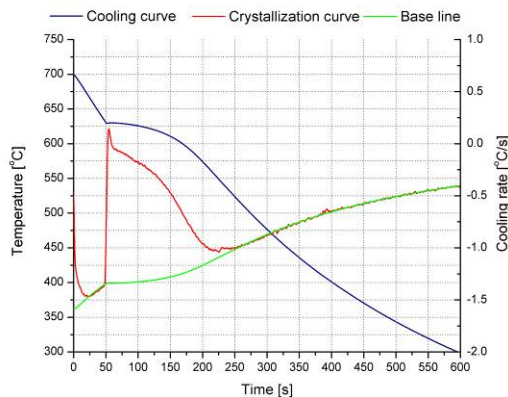
The temperatures of the metallurgical reactions are presented in Table 7. Based on the cooling curve analysis, the non-equilibrium liquidus temperature of MC MgAl3Zn1 was found approximately 631.68°C. At this temperature the first magnesium

dendrites, most likely, nucleated from the melt. Latent heat evolved and caused the temperature of the surrounding melt to rise. This point was clearly visible as a sudden change in the first derivative curve. With further cooling, the magnesium dendrites continued to grow. The formation of the $\alpha(\text{Mg})$ - $\beta(\text{Mg}_{17}\text{Al}_{12})$ eutectic has not been observed. It was found that non-equilibrium solidus temperature was approximately 521.1°C.

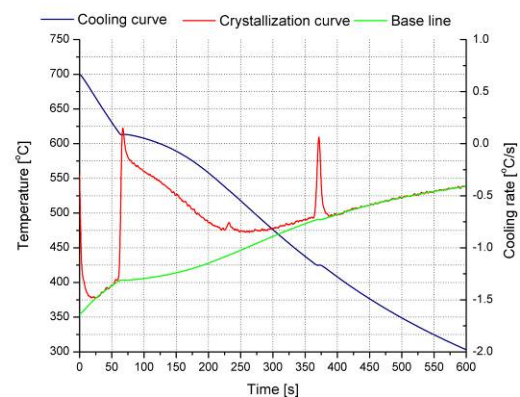
Table 6.
Pointwise chemical composition analysis from Fig. 9.

Analysis	Element	The mass concentration of main elements, %	
		weight	atomic
1	Zn	09.43	03.85
	Mg	60.05	65.95
	Al	30.52	30.20
2	Mg	04.17	06.23
	Al	43.08	58.02
	Si	01.34	01.73
	Mn	51.41	34.01

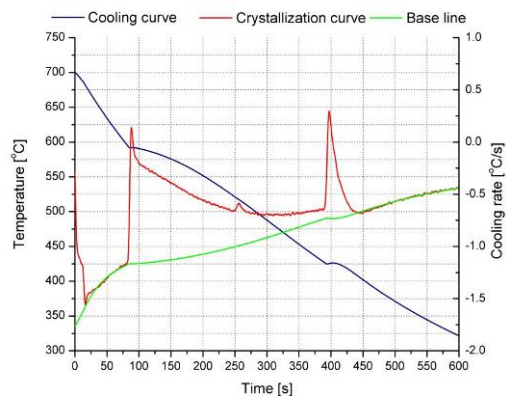
a)



b)



c)



d)

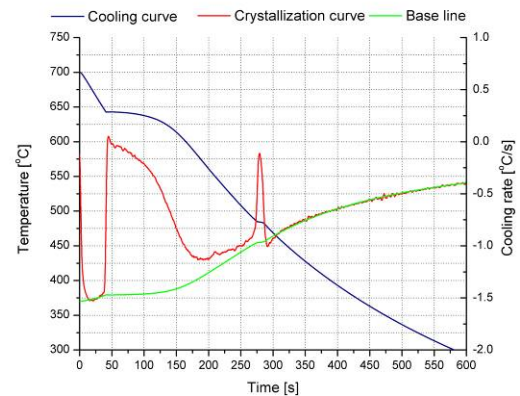


Fig. 9. Cooling and first derivative (cooling rate) vs. temperature curves recorded during the solidification cycles: a) MC MgAl3Zn1, b) MC MgAl6Zn1, c) MC MgAl9Zn1, d) MC MgAl12Zn1

Latent heat of crystallization process of MC MgAl3Zn1 alloy is presented at Table 8. Latent heat of nucleation magnesium dendrites was approximately 1390J, where the latent heat of crystallization process was approximately 1400J.

Based on the cooling curve analysis the non-equilibrium liquidus temperature of MC MgAl6Zn1 was found approximately 622.18°C (Table 9). At 537.85°C the next change in the first derivative curve was observed and corresponded to the precipitate of the phases contained aluminum and manganese and Mg₂Si. Participation of fraction solid at this point was approximately 85% (Table 10). At 427.87°C the next change in the first derivative curve was observed and corresponded to the nucleation of the α(Mg)-β(Mg₁₇Al₁₂) eutectic. It was found that non-equilibrium solidus temperature was approximately 415.98°C, where fraction solid obtained a 100%. Latent heat of crystallization process of MC MgAl6Zn1 alloy is presented at Table 6.

Table 7. Non-equilibrium characteristics of the MC MgAl3Zn1 alloy

Point	Temperature	Time of process	Reaction time	Fs
I	631.68	49.2	0	0
II	629.52	53	3.8	2.1
III	629.84	54.8	5.6	3.93
IV	630.08	58.6	9.4	7.73
V	548.52	225.6	176.4	99.13
VI	530.5	243.4	194.2	99.8
VII				
VIII		Not observed		
IX				
X	521.1	252.8		100

Table 8. Latent heat of crystallization process emitted during solidification and its participation in general latent heat of MC MgAl3Zn1

Specific heat in liquid state Cp _l J/g.°C	Specific heat in solid state Cp _s J/g.°C	Weight g	
1.22	1.015	8.86	
Latent heat of crystallization process			
Reaction	Sample J	Per 1 gram of sample, J/g	Participation %
L→ α(Mg)	1390.56	156.95	99.2
L→ α(Mg)- +Mg ₂ Si+(Al+Mn)	10.41	1.17	0.8
L→ α(Mg)-β(Mg - Mg ₁₇ Al ₁₂)	-	-	-
Sum	1400.96	158.12	100

Table 9. Non-equilibrium characteristics of the MC MgAl6Zn1 alloy

Point	Temperature	Time of process	Reaction time	Fs
I	622.18	56.4	0	0
II	612.72	65.6	9.2	2
III	613.1	67	10.6	3.4
IV	613.41	70	13.6	6.26
V	537.85	225.4	169	85.16
VI	520.58	246.8	190.4	88.86
VII	427.87	363.6	307.2	95.75
VIII	424.85	370.4	314	97.15
IX	425.12	372.4	316	98.21
X	415.98	388.4	332	100

Table 10. Latent heat of crystallization emitted during solidification and its participation in general latent heat of MC MgAl6Zn1

Specific heat in liquid state Cp _l J/g.°C	Specific heat in solid state Cp _s J/g.°C	Weight g	
1.21	1.01	8.99	
Latent heat of crystallization process			
Reaction	Sample J	Per 1 gram of sample, J/g	Participation %
L→ α(Mg)	1258.22	139.96	86.31
L→ α(Mg)- +Mg ₂ Si+(Al+Mn)	143.63	15.98	9.85
L→ α(Mg)-β(Mg - Mg ₁₇ Al ₁₂)	55.98	6.23	3.84
Sum	1457.84	162.16	100

Table 11. Non-equilibrium characteristics of the MC MgAl9Zn1 alloy

Point	Temperature	Time of process	Reaction time	Fs
I	602.76	75.6	0	0
II	591.63	87	11.4	1.54
III	591.85	88	12.4	2.34
IV	592.08	90.6	15	4.4
V	521.41	249.6	174	70.6
VI	510.02	267.8	192.2	74.81
VII	427.31	389.2	313.6	88.44
VIII	424.74	394.8	319.2	89.53
IX	426.35	402.6	327	94.02
X	411.53	436.2	360.6	100

Based on the first derivative of the cooling curve analysis, the liquidus temperature of MC MgAl9Zn1 alloy was found at 602.76°C (Table 11). At this temperature the first crystals of Mg nucleate from the liquid metal. A further decrease in the temperature resulted in formation of the intermetallic phases contained aluminum and manganese and Mg₂Si at 521.41°C. The nucleation of the α(Mg)-β(Mg₁₇Al₁₂) eutectic was observed at 427.31°C. The solidification of alloy finished when the solidus reaction was completed at 411.53°C. Latent heat of crystallization process of MC MgAl9Zn1 alloy is presented at Table 12.

Table 12.

Latent heat of crystallization emitted during solidification and its participation in general latent heat of MC MgAl9Zn1

Specific heat in liquid state Cp _l J/g·°C	Specific heat in solid state Cp _s J/g·°C	Weight g	
1.202	1.002	9.37	
Latent heat of crystallization process			
Reaction	Sample J	Per 1 gram of sample, J/g	Participation %
L → α(Mg)	1180.37	125.97	72.56
L → α(Mg)- +Mg ₂ Si+(Al+Mn)	273.84	29.22	16.83
L → α(Mg)-β(Mg - Mg ₁₇ Al ₁₂)	172.39	18.39	10.59
Sum	1626.6	173.59	100

The non-equilibrium temperatures and latent heat of MC MgAl12Zn1 alloy are presented in Tables 13 and 14. The non-equilibrium liquidus temperature of MC MgAl12Zn1 alloy was found approximately 650.05°C. The formation of the phases contained aluminum and manganese and Mg₂Si was observed at 555.17°C. The nucleation of the α(Mg)-β(Mg₁₇Al₁₂) eutectic was observed at 491.28°C. The solidification sequence of the MC MgAl12Zn1 alloy finished when the solidus reaction was completed at 479.61°C.

Table 13.

Non-equilibrium characteristics of the MC MgAl12Zn1 alloy

Point	Temperature	Time of process	Reaction time	F _s
I	650.05	35.8	0	0
II	642.8	43.2	7.4	2.34
III	642.88	44.8	9	3.85
IV	642.95	47.6	11.8	6.47
V	555.17	205.4	169.6	90.98
VI	543.57	216.2	180.4	91.51
VII	491.28	267.8	232	94.5
VIII	Not observed			
IX				
X	479.61	287.4	251.6	100

Table 14.

Latent heat of crystallization emitted during solidification and its participation in general latent heat of MC MgAl12Zn1

Specific heat in liquid state Cp _l J/g·°C	Specific heat in solid state Cp _s J/g·°C	Weight g	
1.201	1.001	9.04	
Latent heat of crystallization process			
Reaction	Sample J	Per 1 gram of sample, J/g	Participation %
L → α(Mg)	1460.64	161.58	91.74
L → α(Mg)- +Mg ₂ Si+(Al+Mn)	51.76	5.73	3.25
L → α(Mg)-β(Mg - Mg ₁₇ Al ₁₂)	79.8	8.83	5.01
Sum	1592.2	176.13	100

3.2. Heat treatment

During the process of sand casting there have been multicomponent Mg-Al-Zn magnesium cast alloys made with a diversified concentration of alloying components, especially aluminium, as well as Zn and Mn, at a definite plane of micro supplements Pb, Ce, Zr, Sn and Be which ensure obtaining a desirable as-cast and after the heat treatment structure. As a result of thin foils examinations on the transmission electron microscope it has been stated that the structure of a newly worked out, experimental magnesium cast alloy after solution makes a supersaturated solid solution α - Mg with visible dislocation ranges (Fig. 10).

The analysis of thin foils after the process of ageing has validated the fact that the structure of the magnesium cast alloy consists of the solid solution α - Mg (matrix) and an intermetallic secondary phase β - Mg₁₇Al₁₂ in the form of needle precipitations (Fig. 11, 12). The differences of contrasts and the crossing atom bands obtained in high resolution pictures of the solid solution range α constituting the alloy matrix and the intermetallic phase β - Mg₁₇Al₁₂, explicitly indicate a big defect and micro deformations of lattice caused by the heat treatment. Moreover, the examinations of the thin magnesium cast alloy foils after the ageing process confirm the existence of a high density of crystal structure defects identified as a series of straight and parallel dislocations resembling a network. The ageing process has caused the precipitation of evenly distributed dispersive β secondary phase in the needle form that has in the major performed investigations a preferred crystallographic orientation in the matrix. A part of them shows the following relation (Fig. 12):

$$(1\bar{1}01) \alpha\text{-Mg} \parallel (10\bar{1}) \text{Mg}_{17}\text{Al}_{12}$$

$$[11\bar{2}0] \alpha\text{-Mg} \parallel [111] \text{Mg}_{17}\text{Al}_{12}$$

Precipitation of the β - $\text{Mg}_{17}\text{Al}_{12}$ phase are mostly of the shape of roads, and the prevailing growing directions are the directions $\langle 110 \rangle$ α -Mg.

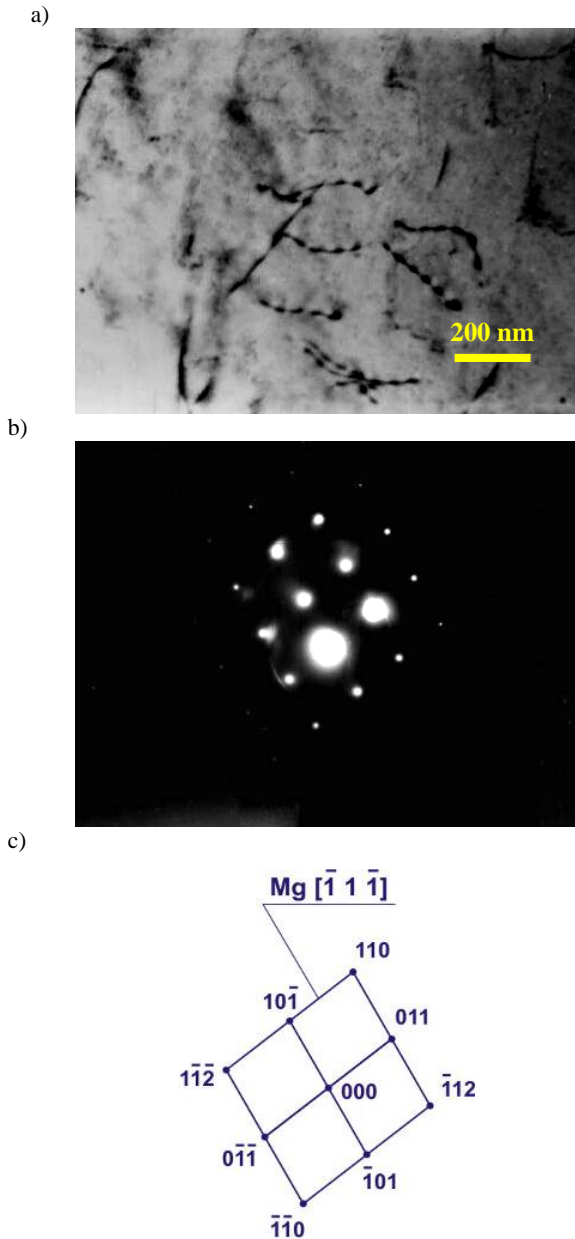


Fig. 10. TEM image of the MCMgAl9Zn1 alloy after solution treatment in the temperature of 430°C for 10 hours with cooling in the water: a) bright field, b) diffraction pattern of area shown in a, c) part of solution for diffraction pattern shown in b

As a result of metallographic investigations made on the light and scanning microscopes it has been confirmed that the magnesium cast alloys in the cast state are characterized by a microstructure of the solid solution α constituting the alloy matrix

as well as the β - $\text{Mg}_{17}\text{Al}_{12}$ discontinuous intermetallic phase in the forms of plates located mostly at grain boundaries. Moreover, in the vicinity of the β intermetallic phase precipitations the presence of the needle eutectics ($\alpha + \beta$) has been revealed (Fig. 13a). In the structure of the examined magnesium cast alloys one can observe, apart from $\text{Mg}_{17}\text{Al}_{12}$ precipitations, turning grey phases, characterized by angular contour with smooth edges in the shape of hexahedrons. Out of the chemical composition examinations with the use of the EDS dispersive radiation spectrometer as well as literature data, one can conclude that it is the Mg_2Si compound which, when precipitating, increases the hardness of castings.

There have appeared, after the process of solutioning with cooling in water and in the air, trace quantities of the β ($\text{Mg}_{17}\text{Al}_{12}$) phase and single precipitations of a light grey phase in the structure of the alloy. There have not been noticed any locations of eutectic occurrences in the structure (Fig. 13b). After the process of solutioning with cooling with furnace the structure of the solid solution α with many precipitations of the secondary phase β has been revealed (locations resembling eutectics). The precipitations of the β ($\text{Mg}_{17}\text{Al}_{12}$) phase, located at grain boundaries and the light grey phase located mostly at the phase β boundary have also been observed. The structure of this alloy is similar to the structure of the as-cast alloy (Fig. 13c). The applied ageing process after the solution heat treatment with cooling in the air has caused the release of the β phase at grain boundaries as well as in the form of pseudo eutectic locations. There have been revealed, in the structure of the material, the parallel twinned crystals extending along the whole grain (Fig. 13d).

As a result of the surface decomposition of elements and the x-ray, quantitative micro analysis made using the EDS energy dispersive radiation spectrometer, the presence of the main alloy additions Mg, Al, Mn, Zn and also Fe and Si included in the magnesium cast alloys in as-cast and after the heat treatment has been confirmed (Fig. 15).

The information about a mass and atom concentration of particular elements in the pointwise examined micro locations of matrix and precipitations. The chemical analysis of the surface element decomposition and the quantitative micro analysis made on the transverse microsections of the magnesium alloys using the EDS system have also confirmed the evident concentrations of magnesium, silicon, aluminium, manganese and iron what suggests the occurrence of precipitations containing Mg and Si with angular contours in the alloy structure as well as phases with high Mn and Al concentrations that are irregular with a non plain surface, often occurring in the forms of blocks or needles. Because the size of particular elements of the structure is, in a prevailing measure, smaller than the diameter of the analyzing beam, the obtained at the quantitative analysis chemical composition may be averaged as a result of which some values of element concentrations may be overestimated. A prevailing participation of magnesium and aluminium and a slight concentration of Zn has been ascertained in the alloy matrix as well as in the location of eutectics and big precipitations that arouse at phase boundaries identified as $\text{Mg}_{17}\text{Al}_{12}$ (Fig. 14, 15).

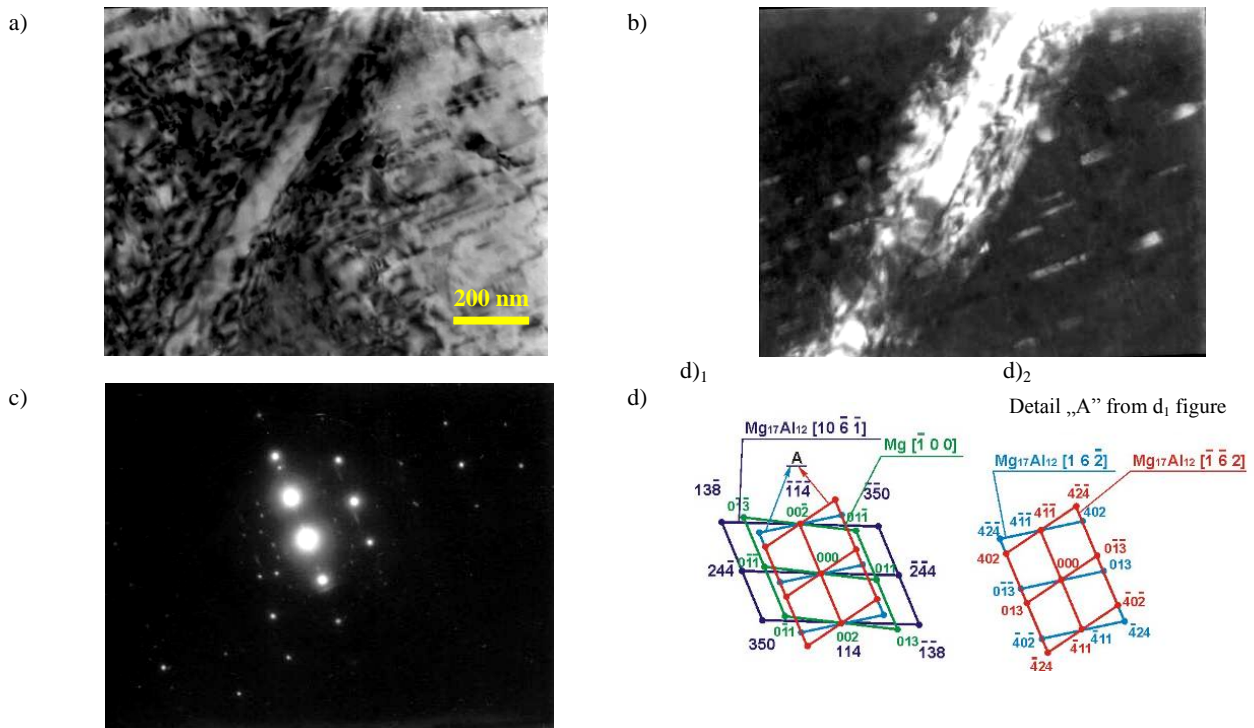


Figure 11. a, b) Bright and dark field (with spot $(\bar{4}0\bar{2})$) image of the MCMgAl9Zn1 alloy after aging treatment with solid solution $\alpha - \text{Mg}$ (matrix) and an intermetallic secondary phase $\beta - \text{Mg}_{17}\text{Al}_{12}$ in the form of needle precipitations, c) diffraction pattern of area shown in a) and b), d₁), d₂) part of solution for diffraction pattern shown in c)

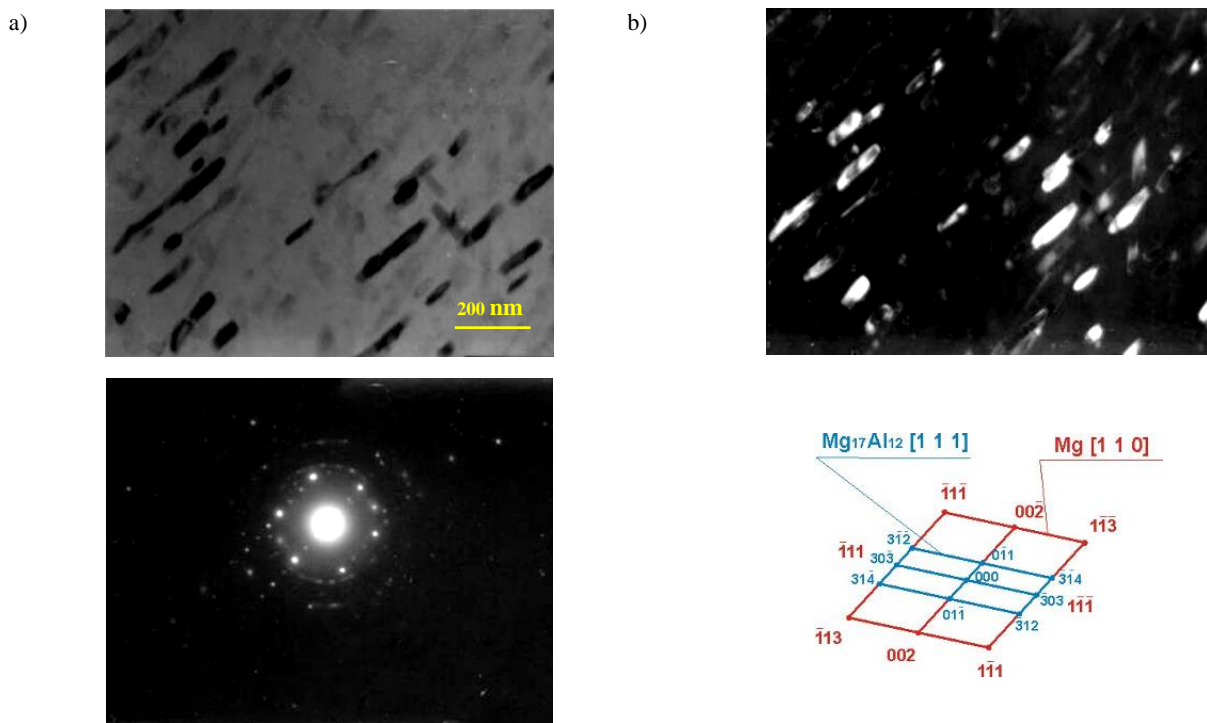


Figure 12. a, b) Bright and dark field (with spot $(\bar{3}\bar{1}4)$) image of the MCMgAl9Zn1 alloy after aging treatment with solid solution $\alpha - \text{Mg}$ (matrix) and an intermetallic secondary phase $\beta - \text{Mg}_{17}\text{Al}_{12}$ in the form of needle precipitations, c) diffraction pattern of area shown in a), d) part of solution for diffraction pattern shown in c)

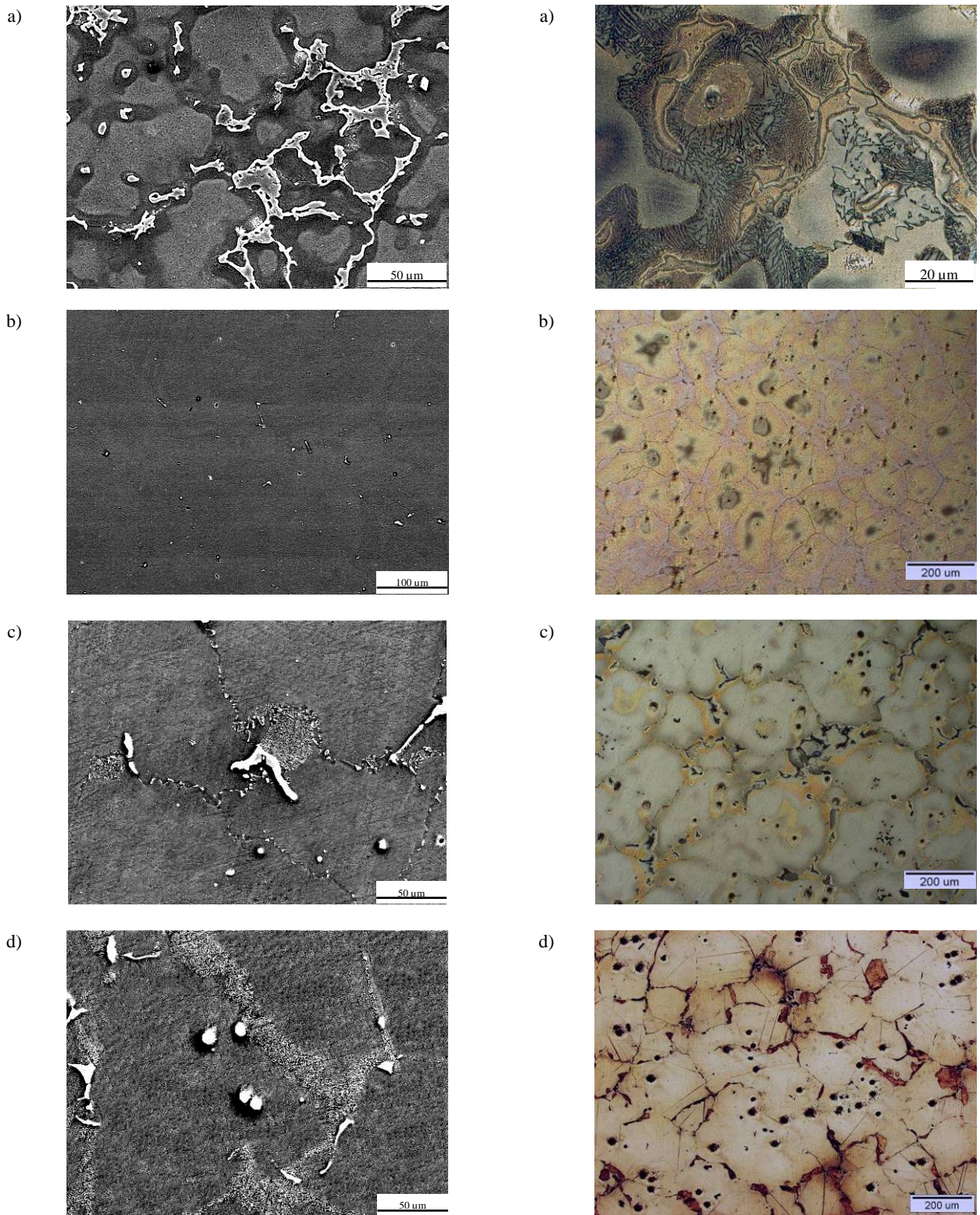


Fig. 13. Microstructure alloys: a) MCMgAl9Zn1 without heat treatment, b) MCMgAl3Zn1 after cooling in the water, c) MCMgAl6Zn1 after cooling with the furnace, d) MCMgAl9Zn1 after aging treatment

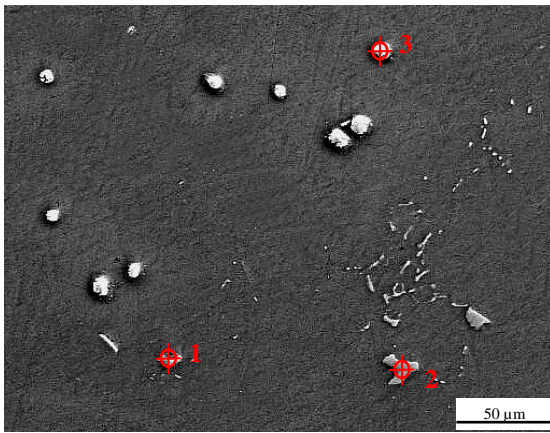


Fig. 14. The X-ray quantitative microanalysis alloy MCMgAl9Zn1, after cooling in the air

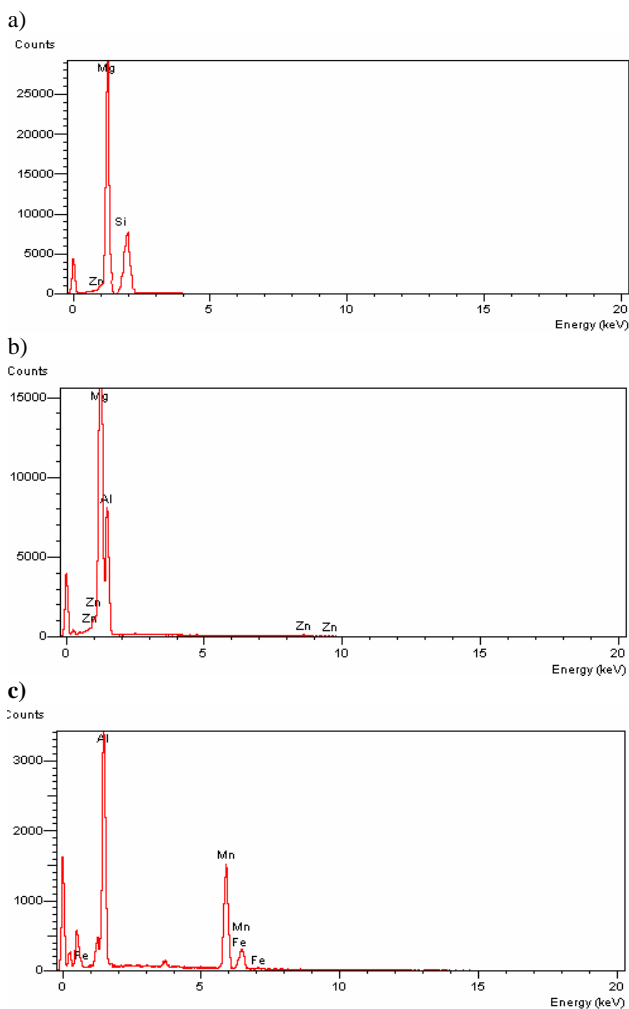


Fig.15. Spectrum of the pointwise chemical composition analysis a)1 (point 1), b) 2 (point 2), c) 3(point 3) from Fig 15

3.3. Mechanical properties

The results of the static tension test make it possible to determine and compare the mechanical and plastic properties of the examined magnesium cast alloys in as cast and after heat-treatment (Fig. 16). On the basis of the tests done, one has stated that the biggest tensile strength in as cast state show the MCMgAl6Zn1 and MCMgAl3Zn1 alloys which also posses the biggest state elongation. It has also been proved that the increase of the Al concentration from 6 to 12% reduces the tensile strength in as cast state. The heat-treatment i.e. the solution heat treatment with the furnace cooling and ageing, causes the increase of the tensile strength. The maximum tensile strength has been obtained after the ageing of the MCMgAl12Zn1 alloy; one has also observed a significant (by 50%) increase of the tensile strength for the MCMgAl9Zn1 specimens after ageing. The smallest growth of the tensile strength after the heat-treatment has been gained for the MCMgAl6Zn1 and MCMgAl3Zn1 materials, 30,3 and 12,4 MPa respectively. The differences in values of the tensile strength for the alloys subjected to solutioning with water and air cooling amount to 6 MPa maximum. Specimens with 12% concentration of aluminum–MCMgAl12Zn1 show a maximum yield point in as cast state (Fig. 16).

The highest value of the yield point after the heat treatment show the MCMgAl12Zn1, MCMgAl9Zn1 and MCMgAl6Zn1 alloys after the solutioning with furnace cooling, insignificantly higher than in the case of the aged materials. The increase of the aluminium concentration to 12% diminishes the elongation of the examined alloys to the value of $2,97\% \pm 0,07$, five times lower in comparison to the elongation of the MCMgAl3Zn cast alloys. The solution heat treatment with water and air cooling causes the increase of the value of elongation even by 100% for MCMgAl12Zn1 and MCMgAl9Zn1 alloys. The alloys after the solution heat treatment with furnace cooling and ageing are characterized by an insignificant fall of the elongation in relation to the as cast state (Fig. 16).

To compare the resistance to wear in conditions simulating the working conditions of the cast magnesium alloys, the abrasive wear investigations have been made in a metal-metal system (Fig. 16). The results of the grindability test done show that the smallest average mass loss in as cast and after the heat treatment at the increasing load from 6 to 12 N is for the MCMgAl12Zn1 alloys. These alloys are characterized by the best tribological properties among the examined materials. Whereas the biggest mass loss for the analyzed cases in the initial state and after the heat treatment has been proved for the MCMgAl3Zn alloy. The biggest as well as the smallest resistance to wear of the examined magnesium alloys, revealed by the average mass loss, corresponds to the results of the hardness of these materials.

Together with the growth of the concentration of aluminium from 3 to 12% in the analyzed alloys, grows their hardness (Fig. 16). The biggest hardness $75,4 \pm 1,15$ HRF in as cast state show the casts from the MCMgAl12Zn1 alloy. It is over two times higher than for the MCMgAl3Zn alloy. Subjecting the material to the heat treatment (solutioning and ageing) has caused the increase of its hardness. The MCMgAl12Zn1, MCMgAl9Zn1 and MCMgAl6Zn1 alloys have reached their highest hardness after the ageing. For the cases after the solution heat treatment,

the hardness insignificantly decreases in comparison to the initial state. For the MCMgAl3Zn casts, the biggest hardness show

specimens after the solutioning with water cooling, and for the remaining cases the hardness results are similar.

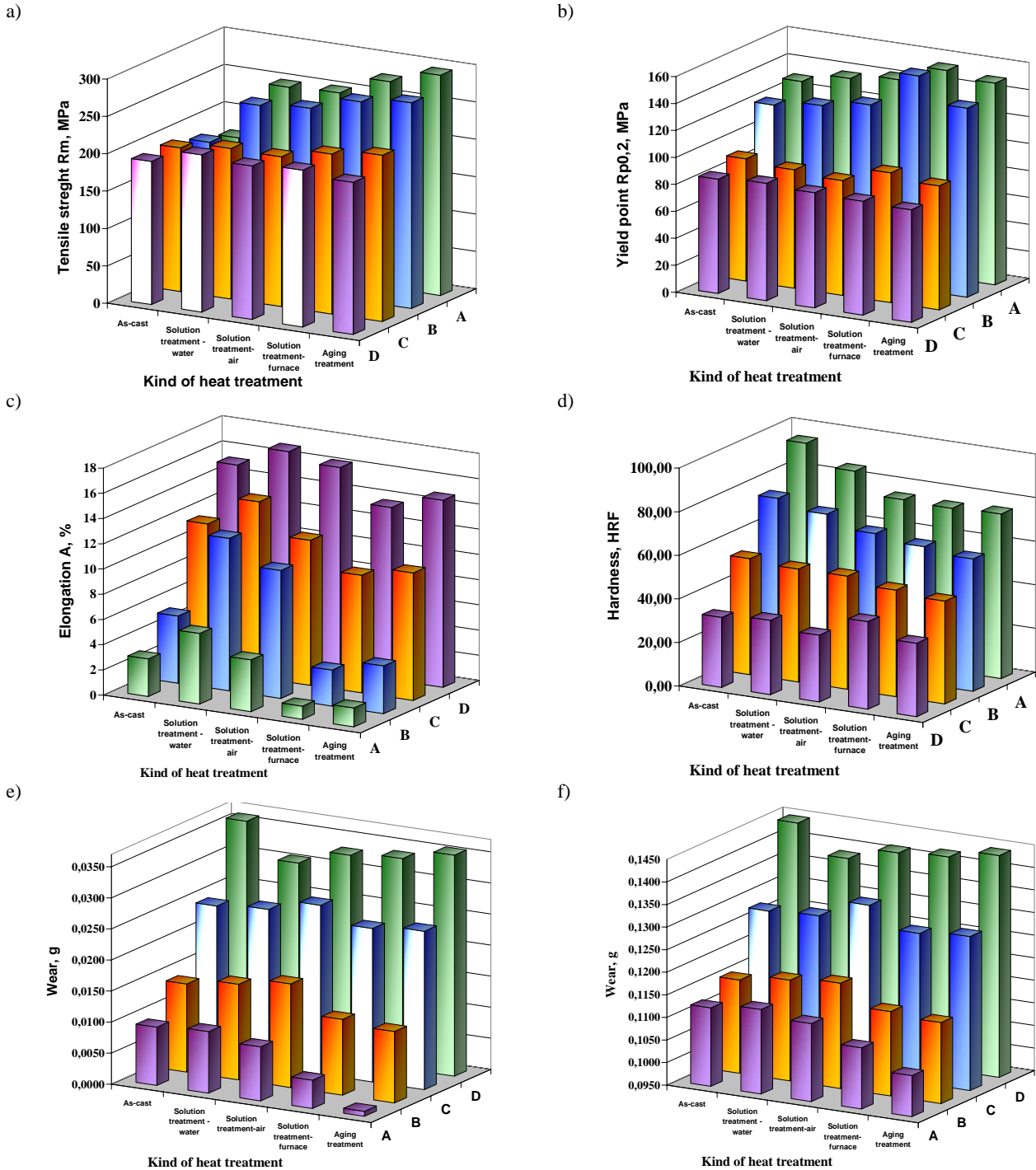


Fig. 16. The results of a) Yield point, b) Tensile strength c) Elongation magnesium casting alloys, d) Hardness, e) Wear resistance test with loads 6 N, f) Wear resistance test with loads 12 N: A) MCMgAl12Zn1, B) MCMgAl9Zn1, C) MCMgAl6Zn1, D) MCMgAl3Zn1

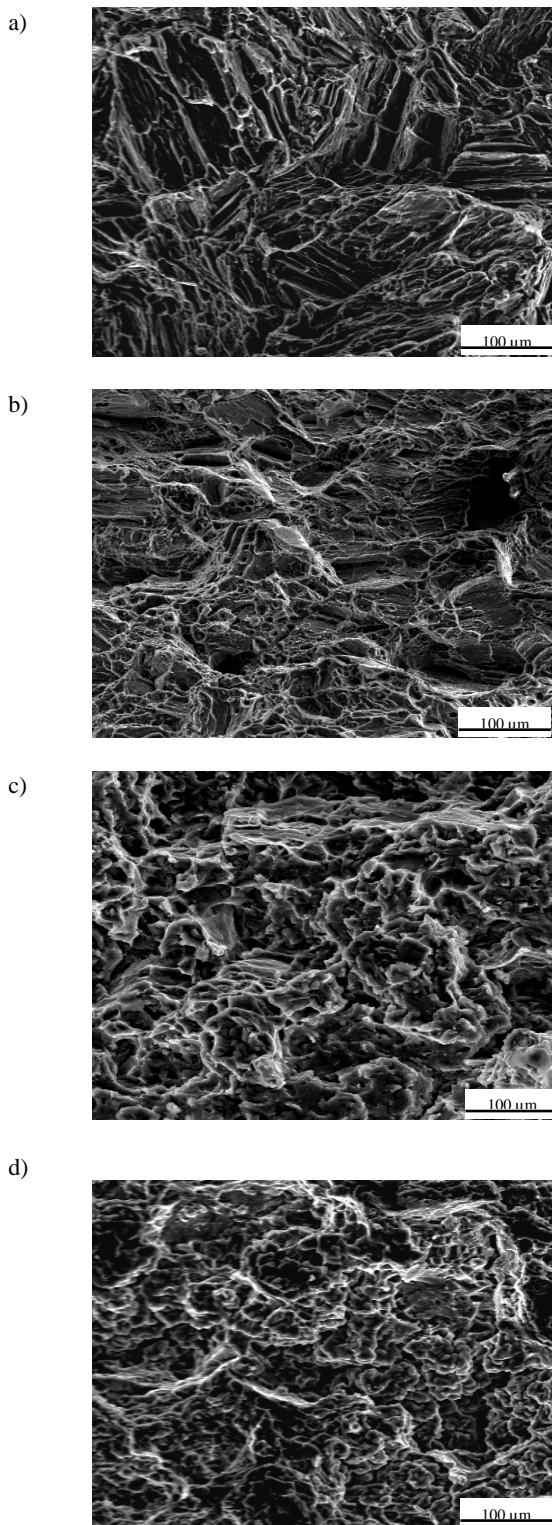


Fig. 17. The fracture surface of tensile test alloys after aging treatment: a) MCMgAl12Zn1 b) MCMgAl9Zn1, c) MCMgAl6Zn1, d) MCMgAl3Zn1

For fuller characteristics of the influence of the heat treatment and the aluminum concentration on the properties of the magnesium cast alloys, the pictures of the structures of fractures after a static test of elongation, have been presented in Figure 17. One of the results of the carried out investigations is the fact that MCMgAl12Zn1, MCMgAl9Zn1 and MCMgAl6Zn1 alloys in as cast state are characterized by a mixed fracture, whereas in the case of the MCMgAl3Zn alloys one can observe a ductile fracture. Subjecting the alloys to the heat treatment consisting in solutioning with water and air cooling, has increased the plasticity of the alloys, which may prove the ductile, in most cases, character of the fracture, and the increase of the contraction and elongation values. The MCMgAl12Zn1 and MCMgAl9Zn1 alloys, in turn, heated and cooled with furnace as well as subjected to ageing, in which a significant increase of hardness in comparison with the initial state and an insignificant lowering of the contraction and elongation values took place, show a brittle fracture character; in the MCMgAl6Zn1 and MCMgAl3Zn alloys the mixed fracture has been observed (Fig. 17).

3.4. Laser treatment

Laser surface modification was conducted by remelting Mg-Al-Zn surface and feeding of carbides or oxides particles. Hard carbides and oxides particles are immediately distributed throughout the molten zone during laser surface melting operation to form the composite layer distributed in alloyed zone.

In the consequence of initial investigations determined powder feed rate, which ensure the most stable feeding, as 8 ± 1 g/min, 7 ± 1 g/min for WC, TiC, VC powders and 4 ± 1 g/min for SiC and Al_2O_3 powder respectively. Different powder feed rate value for each powder is the result of them different density and grain size. In the same initial investigations scan rate was determined as 0.75 m/min for SiC, TiC, WC and also VC powders and as 0.50 m/min for Al_2O_3 powder. This distinction probably is the result of different laser radiation absorption for each powder and each magnesium alloy. The optimization of process parameters was made for the sake of mixture quality, distribution uniformity of alloying particles in the remelted zone and surface geometry after laser alloying.

The cross-section of the microstructure of specimens for the different carbides or oxides particles after laser alloying was shown in Fig. 18. The surface layer consist of the remelting zone, heat affect zone and substrate. It was found that the magnesium alloy with aluminum concentration 3 and 6 wt. % of revealed negligible heat affect zone in opposition to magnesium alloys with aluminum concentration of 9 and 12 wt. %.

The microstructure of the surface layer consists mainly of a dispersion of carbides or oxides particles in the Mg and Al matrix. The structure of the alloyed zone is mainly dendritic of primary magnesium with eutectic of Mg and $Mg_{17}Al_{12}$.

Fig. 19 shows the SEM morphology of the MCMgAl9Zn1 alloy surfaces alloying with TiC, SiC and Al_2O_3 particles. Arrangement of alloying particles in the remelted zone is depended on alloying powder type and laser power. The uniform distribution of the particles after alloying with TiC and WC particles associated may be noted. SiC particles are arranged majority near the surface for high power of laser and only at the surface for low laser power. Al_2O_3 powder particles are located

mainly at the lower area of the remelted zone for all applied laser power. The small amount of VC particles in the alloyed zone was observed.

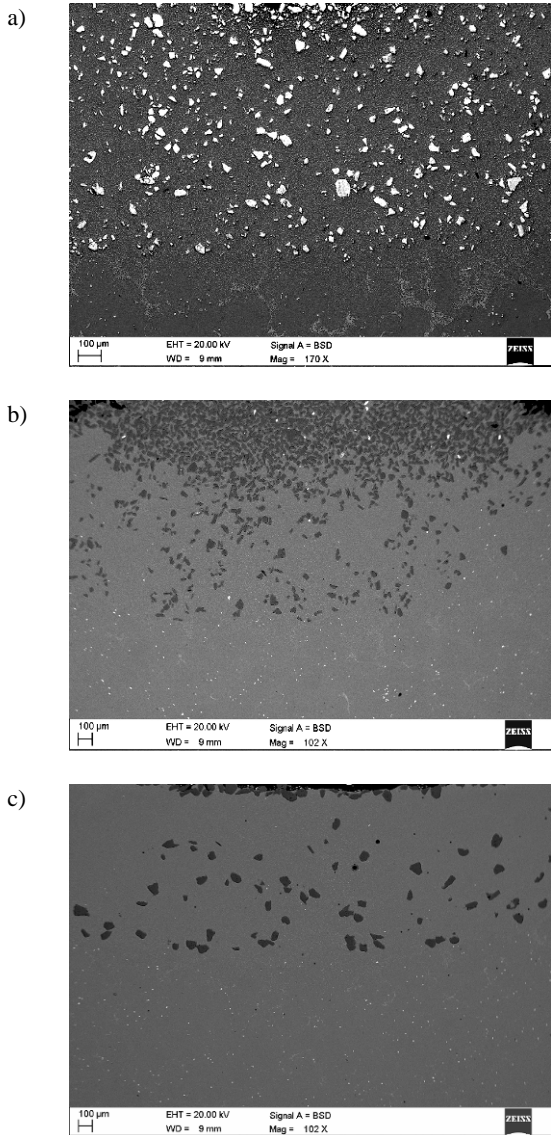


Fig. 18. Scanning electron microscope micrograph of cross-section laser modified surface of the MCMgAl9Zn1 alloy with a) TiC (laser power-1.6 kW), b) SiC (laser power 2.0 kW), c) Al₂O₃ (laser power 2.0 kW) particles

Fig. 20 show the scanning electron micrographs of the interface between modified zone and the substrate of the MCMgAl3Zn1, MCMgAl6Zn1, MCMgAl9Zn1 and MCMgAl12Zn1 alloy with SiC, TiC particle. The interface between the alloying zone and substrate shows good metallurgical joint. The microstructure is characterized by refined grains which are oriented along the direction of heat flow.

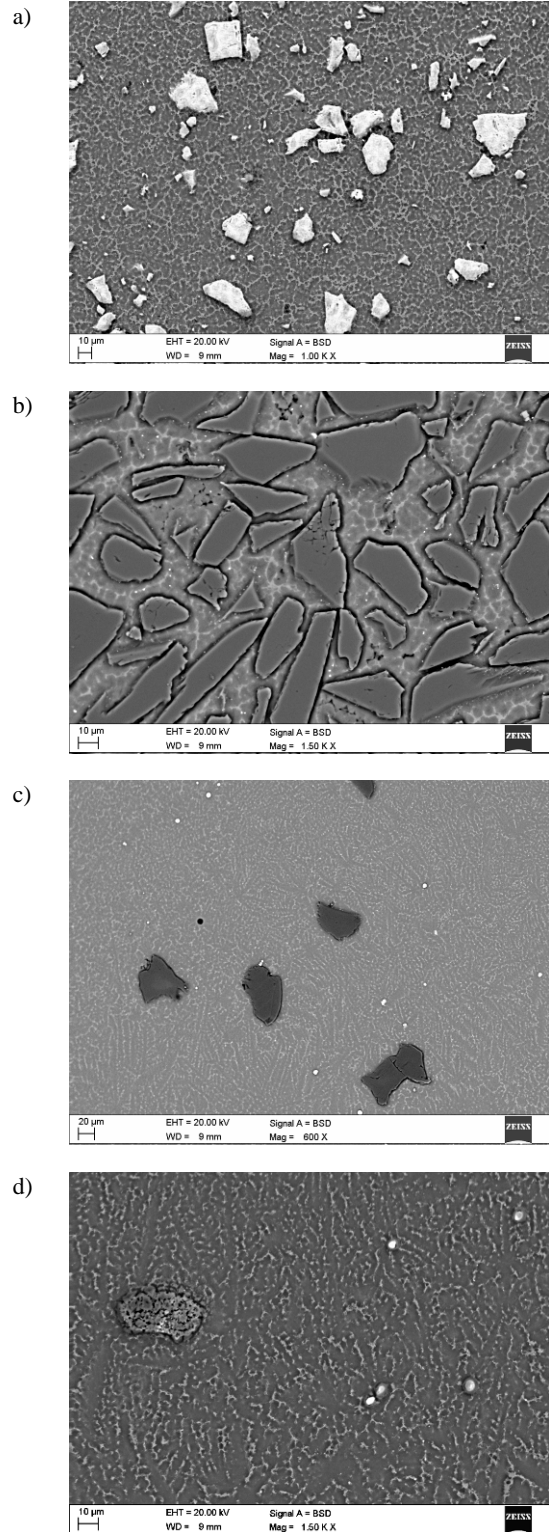


Fig. 19. Scanning electron microscope micrograph of alloyed zone centre of laser modified surface of the MCMgAl9Zn1 alloy with a) TiC, b) SiC, d) Al₂O₃ particles

The refining due to laser surface melting and rapid quenching. The grains of the substrate are significantly coarser than that after laser treatment.

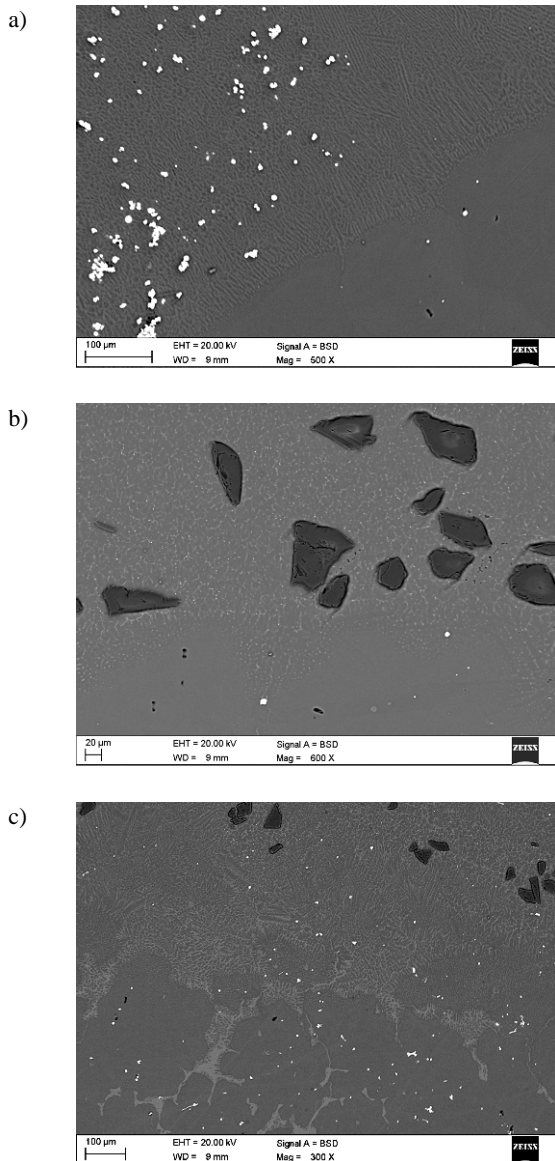


Fig. 20. Scanning electron microscope micrograph of interface between modified zone and the substrate of the: a) MCMgAl3Zn1 alloy with WC particles (laser power-2.0 kW) b) MCMgAl6Zn1 alloy with Al₂O₃ particles (laser power-2.0 kW), c) MCMgAl12Zn1 alloy with SiC particles (laser power 2.0 kW)

Figs. 21-23 show the X-ray diffraction pattern of the laser surface treated Mg-Al-Zn alloys with ceramic particles (Al₂O₃, SiC, WC) consists of presence of Mg-α, Mg₁₇Al₁₂ and peaks using carbides or oxides.

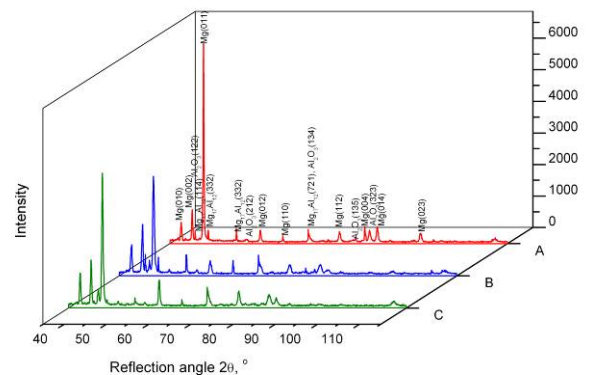


Fig. 21. X ray diffraction pattern of the: ENMCMgAl9Zn1 cast magnesium alloy after laser alloying with Al₂O₃: powder feed rate: 4-5 g/min, scan rate: 0.50 m/min, laser power: A-1.2[kW], B-1.6 [kW], C-2.0[kW]

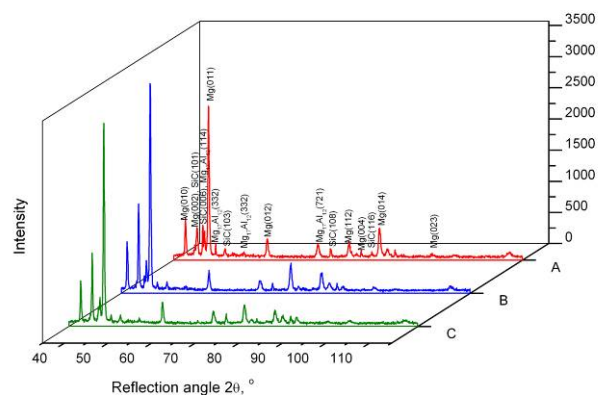


Fig. 22. X ray diffraction pattern of the: ENMCMgAl9Zn1 cast magnesium alloy after laser alloying with SiC: powder feed rate: 8-9 g/min, scan rate: 0.75 m/min, laser power: A-1.2[kW], B-1.6 [kW], C-2.0[kW]

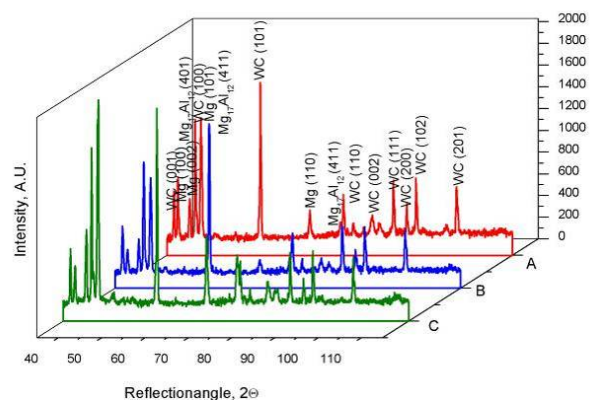


Fig. 23. X ray diffraction pattern of the ENMCMgAl9Zn1 cast magnesium alloy after laser alloying with WC: powder feed rate: 7±1 [g/min], scan rate: 0.75 [m/min], laser power: A-1.2[kW], B-1.6 [kW], C-2.0[kW]

The linear analysis of the chemical composition changes (Fig. 24) and also the chemical analysis (Fig. 25, 26) of the surface element composition and the qualitative microanalysis made on the transverse microsections of the magnesium alloys after laser alloying laser of magnesium alloy with SiC (Fig. 24) (laser power: 2.0 kW, scan rate: 0.75 m/min, powder feed rate: 8 ± 1 g/min), Al_2O_3 powders (Fig. 25) (laser power: 2.0 kW, scan rate: 0.50 m/min, powder feed rate: 7 ± 1 g/min) using the EDS system have confirmed the concentrations

of magnesium, aluminum, manganese, zinc and SiC or Al_2O_3 , respectively. The homogeneous distribution of magnesium and aluminum, except for carbide or oxide particles was observed. Absence of magnesium, aluminum and zinc and occurrence of applied carbide particles in the zone of hard particles, confirms that carbide particles did not melt or dissolve in magnesium matrix.

The adherent particle - matrix and formation of a defect free interface was observed (Fig. 24).

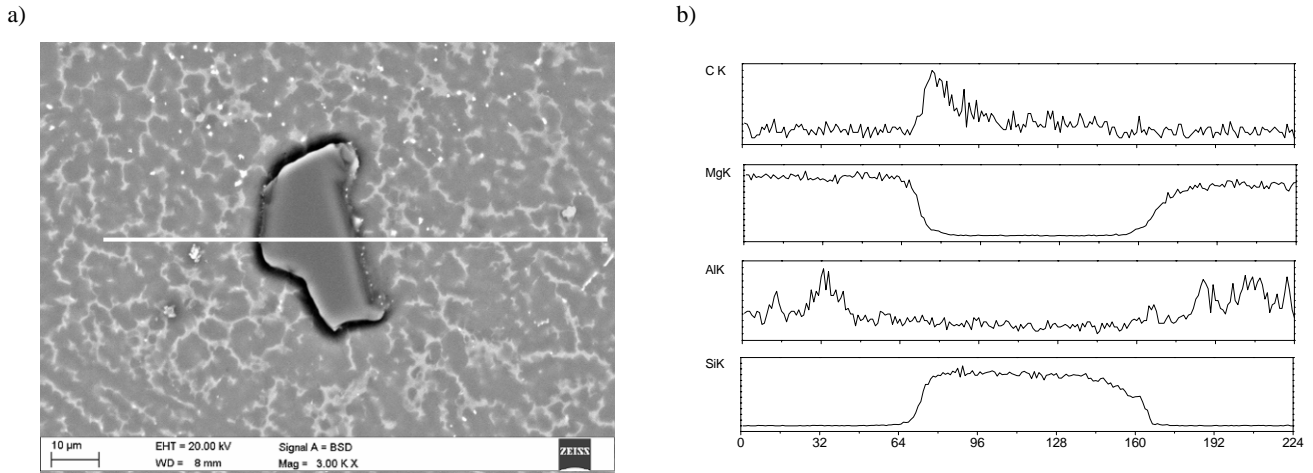


Fig. 24. Scanning electron microscopy micrograph of MCMgAl9Zn1 alloy after laser alloying with SiC particles, laser power: 2.0 kW, scan rate: 0.75 m/min, powder feed rate: 0.75 m/min, a) SEM micrograph, b) linear analysis of the chemical composition changes

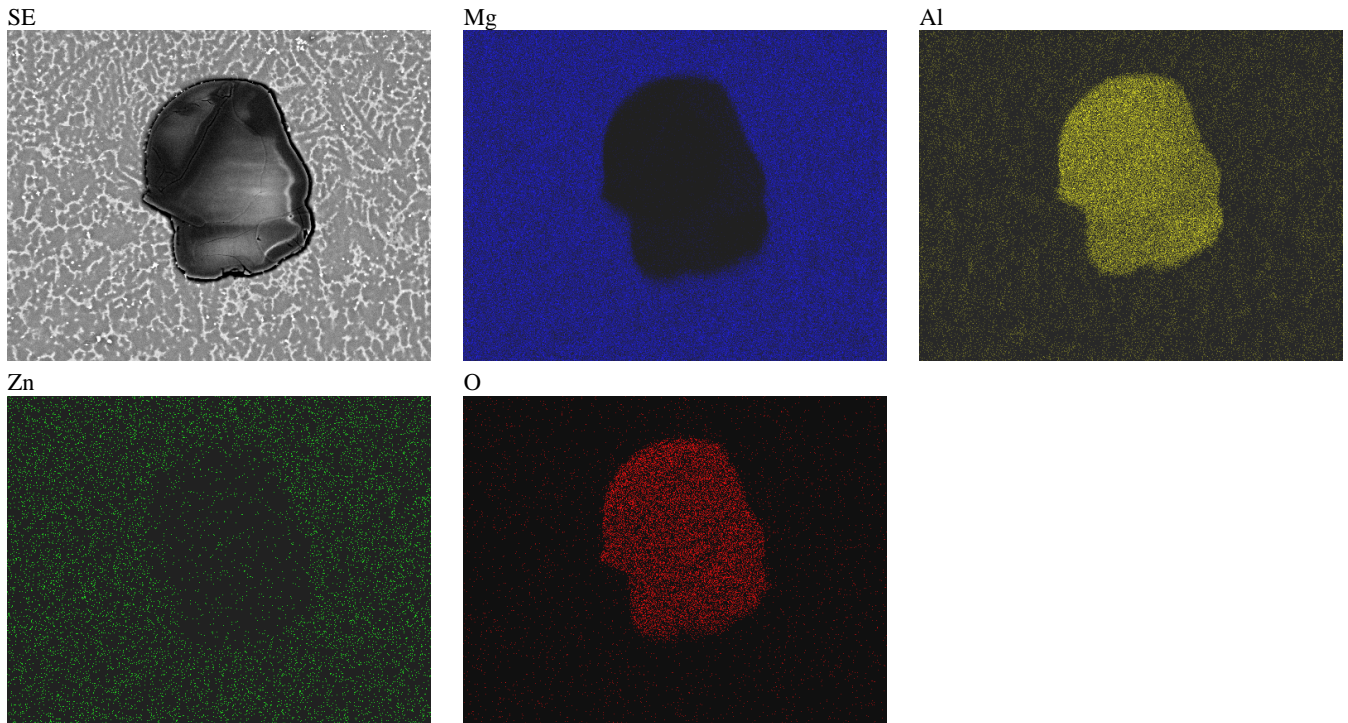


Fig. 25. X-ray mapping of the microstructure EN-MCMgAl6Zn1 alloying layer and the distribution of Mg, Al, Zn, O

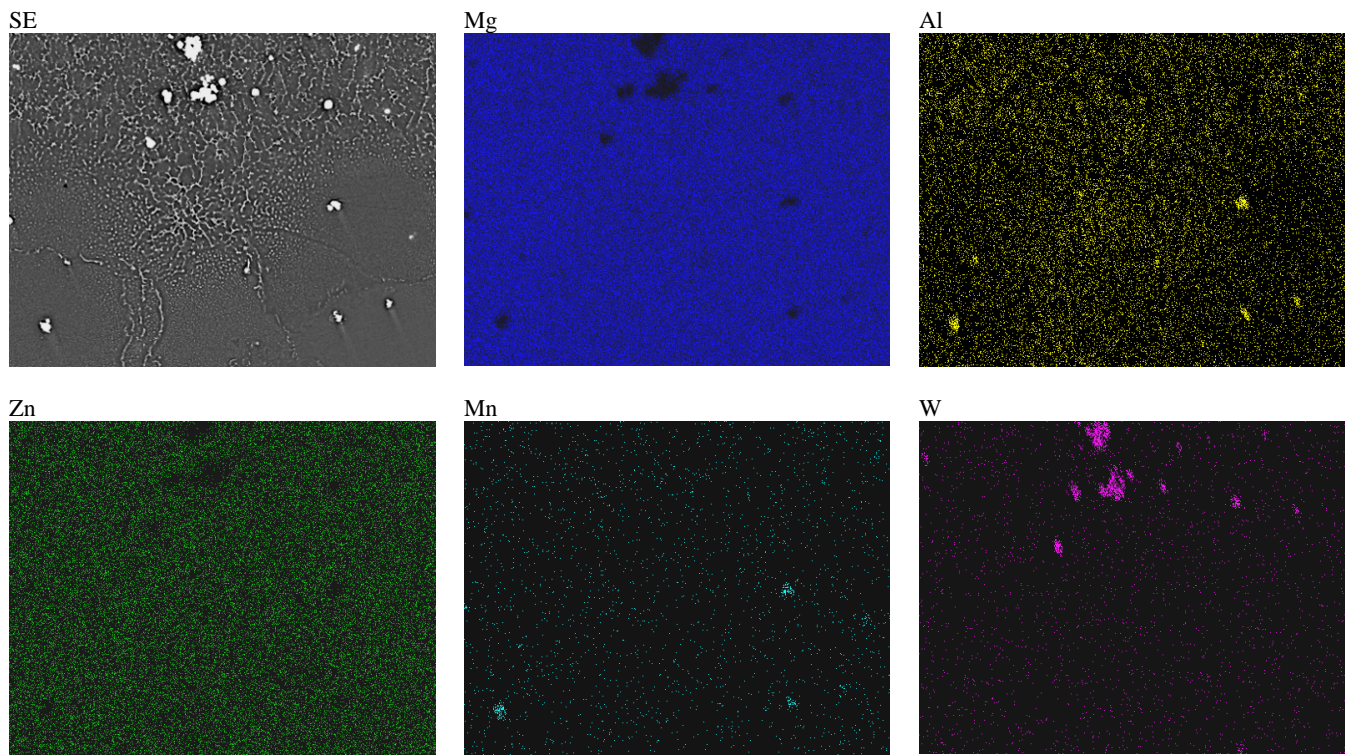


Fig. 26. X-ray mapping of the microstructure EN-MCMgAl6Zn1 alloying layer and the distribution of Mg, Al, Zn, Mn, W

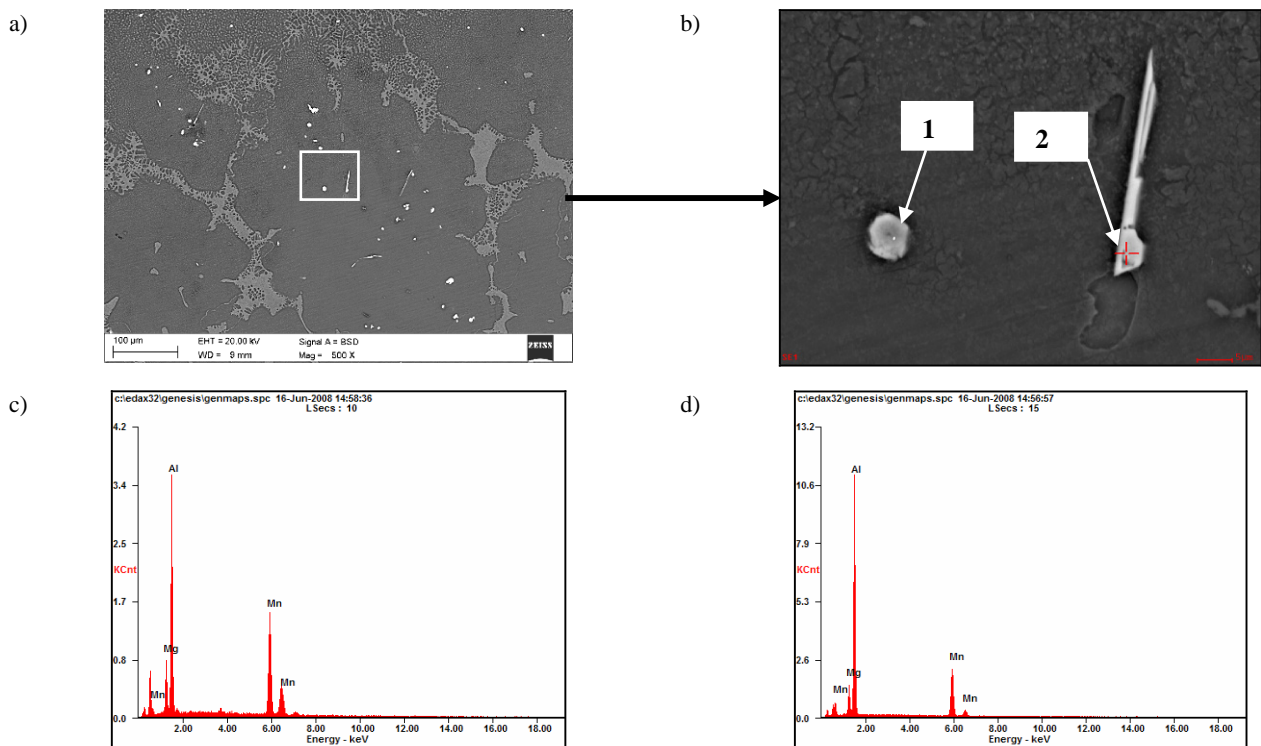


Fig. 27. Scanning electron microscope micrograph of a) the cross-section of laser alloyed MCMgAl9Zn1 alloy, b) magnified view of the boxed region from a), c) analysis from point 1, d) analysis from point 2

Table 15. Summary of EDS analysis of the regions marked in Fig. 28

Region	Element	Wt%	At%
1	MgK	10.23	14.69
	AlK	42.9	55.52
	MnK	46.87	29.79
2	AlK	07.36	09.86
	MnK	57.48	69.32
	MnK	35.15	20.82

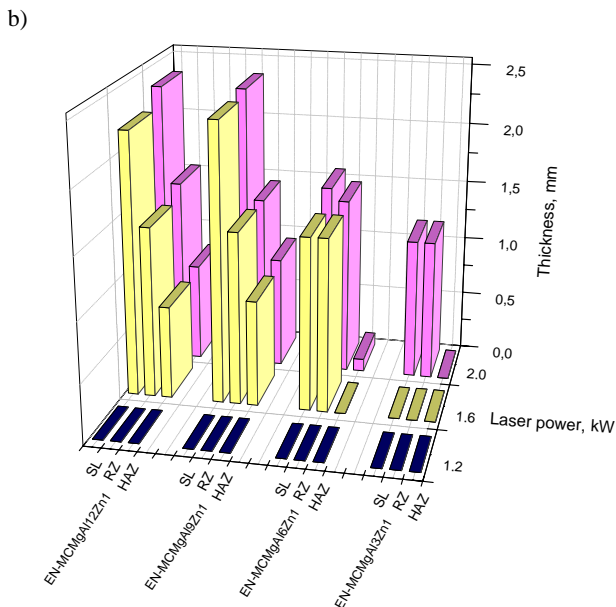
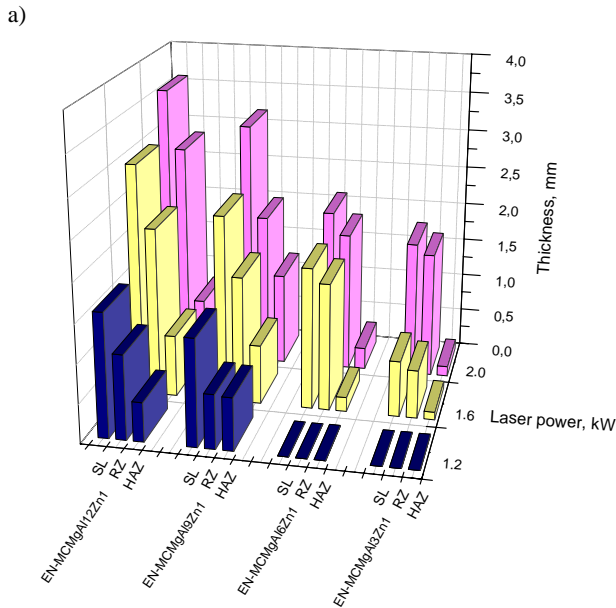


Fig. 28. Diagram of thickness changes of particular areas in surface layers after alloying: a) SiC powder, b) Al₂O₃ powder; SL – surface layer, HAZ – heat affected zone, RZ – remelted zone

Fig. 27 a) shows the cross section view of the laser alloyed surface and Fig 27b) shows the magnified view of the boxed region in Fig. 27a). Fig. 28 c-d show the analysis of chemical composition from point 1 and 2 from Fig 27. Table 15 gives the results of the EDS analysis at various regions marked at 1 and 2. In cast magnesium alloys (Mg-Al), particles containing aluminium and manganese appear. These particles have different forms and sizes. Fig 27b shows the various morphologies on the cast magnesium alloys after laser treatment. This different dimensions and morphology depending on the solidification conditions. The X-ray mapping (Fig. 26) of EN MCMgAl6Zn1 alloy confirm the appears Al-Mn phase in magnesium alloys after laser treatment.

The depth of the surface alloying layer was varied with laser power and also scan rate. Investigated casting magnesium alloys characterize the different laser radiation absorption. Absorption is the highest for MCMgAl12Zn1 alloy and decrease with a decreasing Al concentration in the alloy. In the result a thickness of remelted zone and heat affected zone are changed (Fig. 28).

Fig. 29 shows influence laser power and scan rate on the remelting width of the surface alloying layer after laser treatment. The width of the surface alloying layer was varied with scan rate and also laser power.

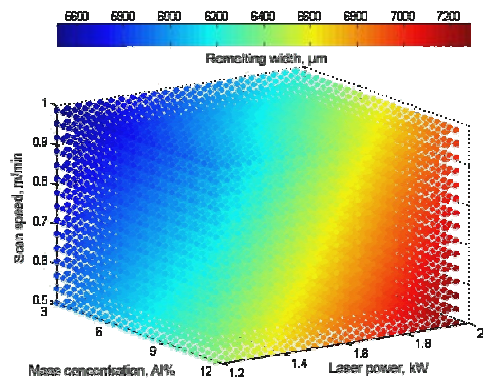


Fig. 29. Graph of the regression function showing dependence of remelting width to aluminium concentration (wt. %), laser power and scan rate

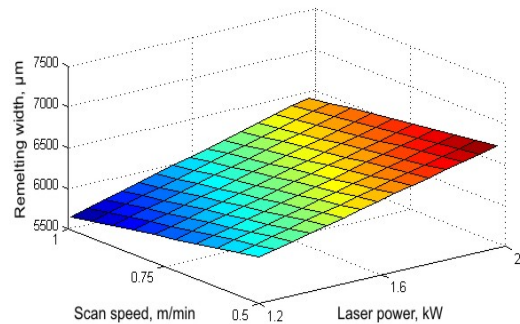


Fig. 30. Graph of the regression function showing dependence of remelting width from laser power and scan rate for the EN-MCMgAl6Zn1 alloy

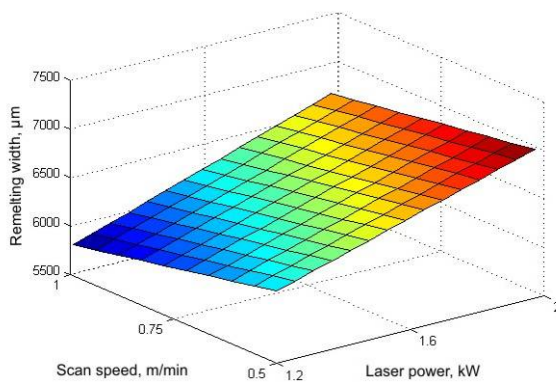


Fig. 31. Graph of the regression function showing dependence of remelting width from laser power and scan rate for the EN-MCMgAl12Zn1 alloy

The width of the surface alloying layer increased with power, mainly because of increasing of the absorbed energy with the laser power, and decreases with an increase in laser scan rate. Fig. 30 and 31 show the graph of the regression function showing dependence remelting width from laser power and scan rate for the MCMgAl6Zn1 and MCMgAl9Zn1, respectively.

The microhardness of the modified surface was measured from the top towards the clad-substrate interface along the cross-sectional plane. Fig. 32-34 show the microhardness curves of the cross-section of the coating. The microhardness of the modified zone is increased as compared to that of as-received Mg alloy, due to the enhancement of hard particles and also the grain refinement has positive effect on the improvement of the microhardness (80-250 HV_{0.1}). There is the little fluctuation in the readings in some region, possibly because of the random distribution of hard particles in the surface modified layer. In case, when penetration take place in hard carbides or oxide particle microhardness (about 1400 - 1600 HV_{0.1}) is much bigger than the measures were from matrix.

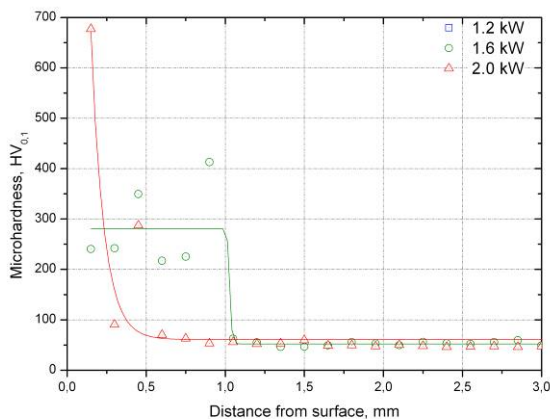


Fig. 32. Cross-section microhardness profile from the surface MCMgAl3Zn1 alloy with SiC particles, scan rate: 0.75m/min

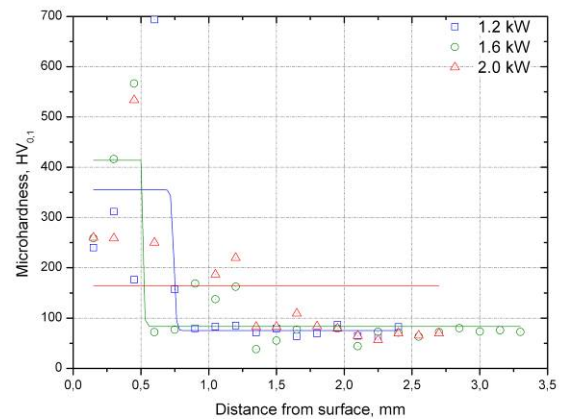


Fig. 33. Cross-section microhardness profile from the surface MCMgAl9Zn1 alloy with SiC particles, scan rate: 0.75m/min

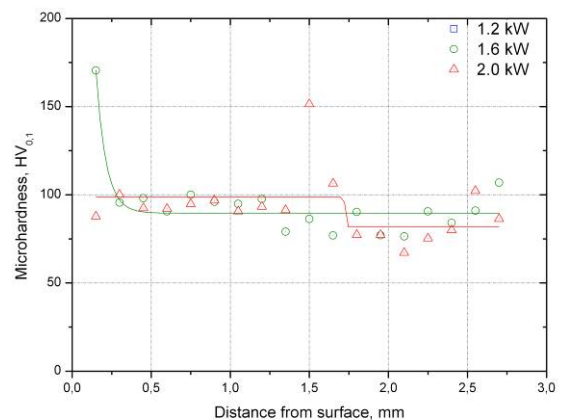


Fig. 34. Cross-section microhardness profile from the surface MCMgAl12Zn1 alloy with Al₂O₃ particles, scan rate: 0.50m/min

It was observed that the microhardness of the remelting zone is higher than that of the heat affect zone. It is due to cooling rate of remelting zone, which has a high cooling rate.

3.5. Neural network model

The data set has been obtained from the examinations of the hardness of magnesium cast alloys after solution heat treatment (water, air) and annealing in 400, 415 and 430 °C temperatures in the time of 10, 20 and 30 hours, and also after ageing with air-cooling in temperatures between 150 and 210 °C and in the time of 5, 10 and 15 hrs.

The data for the solution heat treatment and ageing has been divided randomly into three subsets: learning, validating and testing ones. In case of the network calculating the hardness after solutioning, the number of cases was adequately 68, 20 and 20, whereas for the network calculating the hardness after ageing was 231, 100 and 101. The data from the learning set has been used

for the modification of the network weights, the data from the validating set, to evaluate the network during the learning process, while the remaining part of the values (the testing set) has been used for determining the network efficiency after ending completely the procedure of its creating.

The results used in the learning process and the network testing have been put to standardization. Scaling has been used in relation to the deviation from the minimal value, according to the mini-max function. The mini-max function transforms the variable domain to the range (0,1). The type of the network, the number of neurons in the hidden layer (layers), the method and learning parameters have been determined observing the influence of these quantities onto the assumed network quality coefficients.

The quotient of standard deviations for errors and the data has been accepted, as the vital indicator of the model quality, made with the use of the neural network. The correctness of the network model may only be considered in case when the presented by

networks forecasts are burdened with a smaller error than the simple estimation of the unknown output value.

For both, the networks calculating the hardening after the solution heat treatment as well as after ageing, as the optimal has been recognized the MLP unidirectional network (multilayer perceptron) with one hidden layer and 5 neurons in the layer. The error function in the form of the sum square has been accepted together with the logistic activation function.

The learning method based on the conjugate gradient algorithm has been applied, representing the examples from the learning set for 101 training patterns for the network calculating the hardness after solution heat treatment, and 195 patterns for the network calculating the hardness after ageing.

On the basis of the worked out models of neural networks, the diagrams of the influence of the temperature and solutioning and ageing times have been done, as well as the aluminum content onto the hardness of the analyzed magnesium cast alloys (Fig. 35).

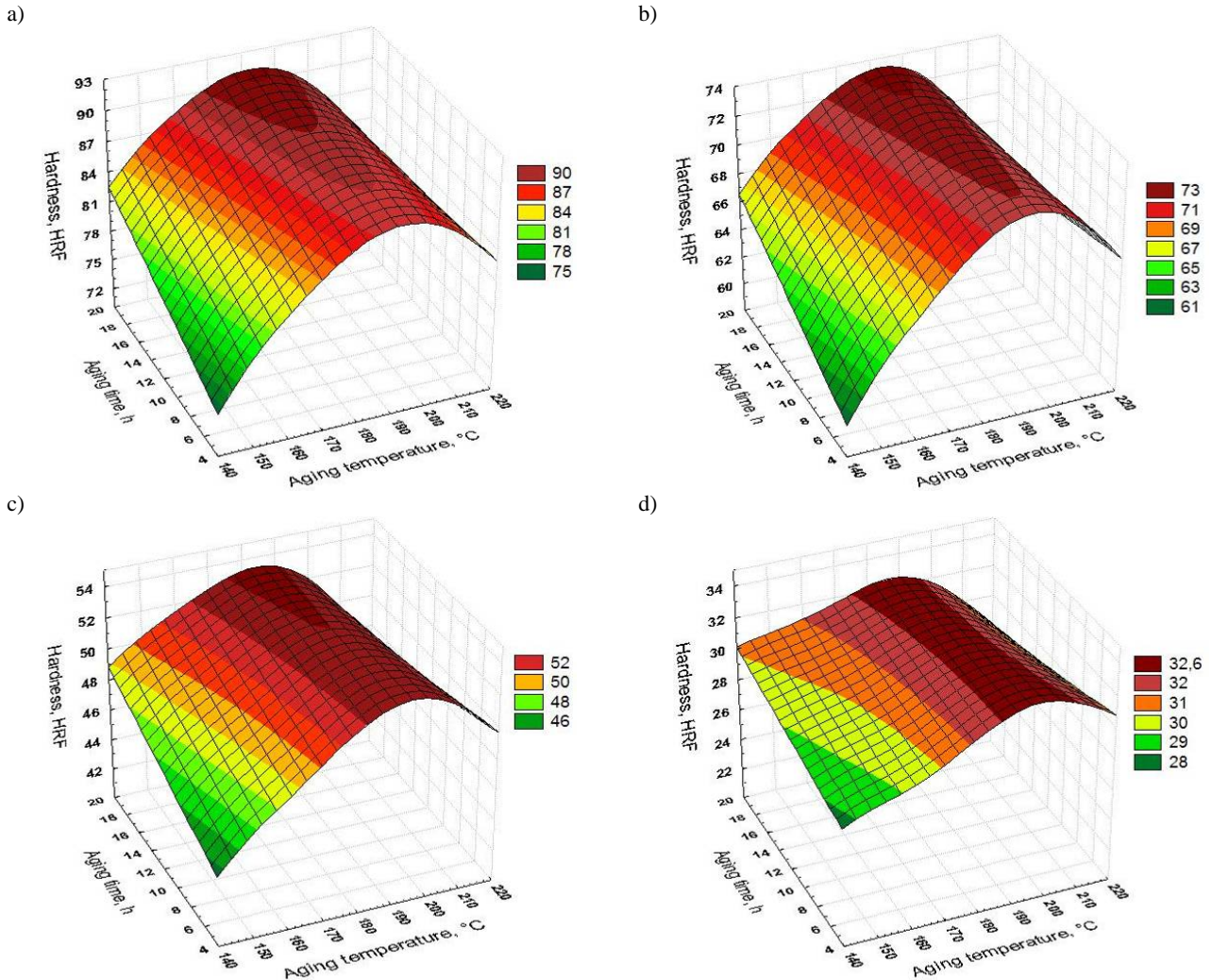


Fig. 35. Simulation of the temperature and ageing time influence on hardness of the cast magnesium alloys by selected solution treatment temperature and time - 430°C and 10 hours

4. Summary

The analysis of the thin foils after the ageing process has confirmed that the structure of the magnesium cast alloy consists of the solid solution α – Mg (matrix) of the secondary phase β – $\text{Mg}_{17}\text{Al}_{12}$ evenly located in the structure. The structure creates agglomerates in the form of needle precipitations, partially coherent with the matrix placed mostly at the grain boundaries. Precipitation of the β - $\text{Mg}_{17}\text{Al}_{12}$ phase are mostly of the shape of rods, and the prevailing growing directions are the directions $\langle 110 \rangle$ α -Mg. The chemical analysis of the surface element decomposition and the quantitative micro analysis made on the transverse microsections have confirmed the evident concentrations of magnesium, silicon, aluminium, manganese and iron what suggests the occurrence of precipitations containing Mg and Si with angular contours, as well as phases with high Mn and Al concentrations that are irregular, with a non plain surface, often occurring in the forms of blocks or needles.

Precipitation hardening causes some changes in the properties. The biggest tensile strength in as cast state show the MCMgAl6Zn1 and MCMgAl3Zn alloys, $192,1 \pm 1,95$ and $191,3 \pm 1,6$ MPa respectively. They also have the biggest elongation in as cast state. It has also been proved that the increase of the Al concentration from 6 to 12% lowers the tensile strength in as cast state to $170,9 \pm 1,64$ MPa. The maximum tensile strength has been obtained after the ageing of the MCMgAl12Zn1 alloy; one has also observed a significant (by 50%) increase of the tensile strength for the MCMgAl9Zn1 specimens after ageing. The biggest value of the yield point after the heat treatment show the MCMgAl12Zn1 , MCMgAl9Zn1 and MCMgAl6Zn1 alloys after the solutioning with furnace cooling, insignificantly higher than in the case of the aged materials.

Together with the growth of the concentration of aluminum from 3 to 12% in the analyzed alloys, grows their hardness. The biggest hardness $75,4 \pm 1,15$ HRF in as cast state show the casts from the MCMgAl12Zn1 alloy.

The obtained results show that the carried out heat treatment of the investigated materials causes the increase of their resistance to abrasive wear.

The obtained results explicitly indicate that the most favorable type of the heat treatment in terms of the optimal working conditions and the energy used and the time needed for carrying out the solution heat treatment and ageing, and also in terms of the obtaining the best possible mechanical properties, is the solutioning in the temperature of 430°C for 10 hours and ageing in the temperature of 190°C for 15 hours.

The subject of the research is conducted with the evaluation of the influence of the crystallization cooling rate on the phase crystallization temperature in magnesium alloys. The research show that the thermal analysis carried out on UMSA Technology Platform is an efficient tool for collect and calculates data about temperature and time of phase transformations, FS measurements, liquidus and solidus temperatures as well.

The present work revealed a significant difference of up to 23°C that exists between non-equilibrium solidus temperatures based on the solidification cycle. This information is very important for the scientific selection of the optimum solution treatment temperature. Most of the thermal analysis data available in the technical literature pertains to equilibrium and semi-

equilibrium solidification conditions. This data can be useful for limited optimization of the solidification processes. Comparing the results in the present investigation, it can be confirmed that all phases detected by thermal analysis were identified using optical or electron microscopy.

The results of investigations indication that laser treatment of cast magnesium alloys EN-MCMgAl3Zn1 , EN-MCMgAl6Zn1 , EN-MCMgAl9Zn1 , EN-MCMgAl12Zn1 with carbides and aluminium oxide powders is feasible. However, as a result of different properties of each cast magnesium alloys and each applicable powders is necessary to determine process parameters.

The interface between the alloying zone and substrate shows good metallurgical joint. The structure of the remelted zone is mainly dendritic of primary magnesium with eutectic of Mg and $\text{Mg}_{17}\text{Al}_{12}$. The uniform distribution of the particles associated may be noted for WC, VC and TiC powders. Magnesium alloys with aluminium concentration 9 and 12 wt. % reveal heat affected zone in opposition to alloys with aluminium concentration 3 and 6 wt. %.

Results of microhardness investigation show that hardness increase in the remelted zone (values from 100 to 600 $\text{HV}_{0,1}$) compare to substrate material (50-90 $\text{HV}_{0,1}$).

Notice

In the framework of the subject matter described in the given paper Prof. L.A. Dobrzański gave an invited lecture at the 18th Brazilian Congress on Materials Science and Engineering CBECIMAT 2008, Porto de Galinhas, Brazil taking place on 24-28.11.2008 and an invited lecture at the 9th Global Congress on Manufacturing and Management GCOMM 2008, Holiday Inn, Surfers Paradise, Australia taking place on 12-14.11.2008.

Acknowledgements

This scientific work is fragmentary financed within the framework of scientific financial resources in the period 2007-2008 as a research and development project R15 0702 headed by Prof. L.A. Dobrzański.

The authors would like to thank Dr M. Kasprzak, Dr A. Lisiecki and Dr D. Janicki from the Silesian University of Technology in Poland for their help in the realisation of trials of laser melting and thermal analysis.

References

- [1] K.U. Kainer, *Magnesium – Alloys and Technology*, Wiley-VH, Weinheim, Germany, 2003.
- [2] H. Friedrich, S. Schumann, Research for a "New age of magnesium in the automotive industry", *Journal of Materials Processing Technology* 117 (2001) 276-281.
- [3] A. Fajkiel, P. Dudek, G. Sęk-Sas, *Foundry engineering XXI c. Directions of metallurgy development and light alloys casting*, Publishers Institute of Foundry Engineering, Krakow 2002.

- [4] X. Ming-Xu, Z. Hong-Xing, Y. Sen, L. Jian-Guo, Recrystallization of preformed AZ91D magnesium alloys in the semisolid state, *Materials and Design* 26 (2005)343-349.
- [5] E.F. Horst, B.L. Mordike, *Magnesium Technology. Metallurgy, Design Data, Application*, Springer-Verlag, Berlin Heidelberg 2006.
- [6] Kielbus, T. Rzychoń, R. Cibis, Microstructure of AM50 die casting magnesium alloy, *Journal of Achievements in Materials and Manufacturing Engineering* 18 (2006) 135-138.
- [7] J. Zhang, Z.X. Guo, F. Pan, Z. Li, X. Luo, Effect of composition on the microstructure and mechanical properties of Mg-Zn-Al alloys, *Materials Science & Engineering A* 456 (2007) 43-51.
- [8] L.A. Dobrzański, T. Tański, L. Čížek, Z. Brytan, Structure and properties of the magnesium casting alloys, *Journal of Materials Processing Technology* 192-193 (2007) 567-574.
- [9] T. Tański, L.A. Dobrzański, L. Čížek, Influence of heat treatment on structure and properties of the cast magnesium alloys, *Journal of Advanced Materials Research* 15-17 (2007) 491-496.
- [10] S.G. Shabestari, M. Malekan, Thermal analysis study of the effect of the cooling rate on the microstructure and solidification parameters of 319 aluminum alloy, *Canadian Metallurgical Quarterly* 44/3 (2005) 305-312.
- [11] L. Backuerud, G. Chai, J Tamminen, *Solidification characteristics of aluminum alloys Vol. 2 Foundry Alloys*, AFS Skanuminium, Stockholm, Sweden 1990.
- [12] L.A. Dobrzanski, W. Kasprzak, M. Kasprzak, J.H. Sokolowski, A Novel Approach to the Design and Optimization of Aluminum Cast Component Heat Treatment Processes using Advanced UMSA Physical Simulations, *Journal of Achievements in Materials and Manufacturing Engineering* 24/2 (2007) 139-142.
- [13] D. Emadi, L.V. Whiting, S. Nafisi, R. Ghomashchi, Applications of thermal analysis in quality control of solidification processes, *Journal of Thermal Analysis and Calorimetry* 81 (2005) 235-242.
- [14] L.A. Dobrzanski, W. Kasprzak, J. Sokolowski, R. Maniara, M. Krupiński, Applications of the derivation analysis for assessment of the ACAISi7Cu alloy crystallization process cooled with different cooling rate, *Proceedings of the 13th Scientific International Conference on Achievements in Mechanical and Materials Engineering, AMME'2005, Gliwice - Wisla, 2005*, 147-150.
- [15] J.H. Sokolowski, M.B. Djurdjevic, Ch.A. Kierkus, D.O. Northwood, Improvement of 319 aluminum alloy casting durability by high temperature solution treatment, *Journal of Materials Processing Technology* 109 (2001) 174-180.
- [16] H. Yamagata, H. Kurita, M. Aniolek, W. Kasprzak, J.H. Sokolowski, Thermal and metallographic characteristics of the Al-20% Si high-pressure die casting alloy for monolithic cylinder blocks, *Journal of Materials Processing Technology* 199 (2008) 84-90.
- [17] W.T. Kierkus, J.H. Sokolowski, Recent Advances in CCA:A new method of determining baseline equation, *AFS Transactions* 1999 (66) 161-167.
- [18] M.B. Djurdjevic, W.T. Kierkus, G.E. Byczynski, T.J. Stockwell, J.H. Sokolowski, Modeling of fraction solid for 319 aluminum alloy, *AFS Transactions* 14 (1999) 173-179.
- [19] "Method and Apparatus for Universal Metallurgical Simulation and Analysis" – United States Patent, Patent No.: US 7,354,491 B2, Date of Patent: Apr. 8.
- [20] W. Kasprzak, J.H. Sokolowski, W. Sahoo, L.A. Dobrzanski, Thermal and structural characteristics of the AZ50 magnesium alloy, *Journal of Achievements in Materials and Manufacturing Engineering* 29/2 (2008) 179-182.
- [21] H. Yamagata, W. Kasprzak, M. Aniolek, H. Kurita, J.H. Sokolowski, The effect of average cooling rates on the microstructure of the Al-20%Si high pressure die casting alloy used for monolithic cylinder blocks, *Journal of Materials Processing Technology* 203 (2008) 333-341.
- [22] R. MacKay, M. Djurdjevic, J.H. Sokolowski, The effect of cooling rate on the fraction solid of the metallurgical reaction in the 319 alloy, *AFS Transaction*, 2000.
- [23] *Universal Metallurgical Simulator and Analyzer (UMSA) Platform for the Advanced Simulation of Melting and Solidification Processes*, Software Information, 2002.
- [24] L.A. Dobrzański, K. Labisz, M. Piec, A. Klimpel, Modelling of surface layer of the 31CrMoV12-18 tool steel using HPDL laser for alloying with TiC powder, *Journal of Achievements in Materials and Manufacturing Engineering* 24 (2007) 27-34.
- [25] D. Dube, M. Fiset, A. Couture, I. Nakatsugawa, Characterization and performance of laser melted AZ91D and AM60B, *Materials Science and Engineering A* 299 (2001) 38-45.
- [26] F. Vollertsen, K. Partes, J. Meijer, State of the art of Laser Hardening and Cladding, *Proceedings of the 3th International WLT-Conference on Lasers in Manufacturing 2005, Munich*.